



**University of
Zurich**^{UZH}

Reconstructing Rockfall Activity from Deposits on the Witenwasserengletscher (UR) and Investigating the Relationship to Climate Factors

GEO 511 Master's Thesis

Author

Leonora Seiler
18-718-577

Supervised by

Prof. Dr. Andreas Vieli
Florian Hardmeier

Faculty representative

Prof. Dr. Andreas Vieli

29.04.2024

Department of Geography, University of Zurich

Acknowledgments

First and foremost, I want to thank my main supervisor Prof. Dr. Andreas Vieli for supporting me through the whole work, without him this work would not have been possible. Second, I would like to express my thanks to Florian Hardmeier, my co-supervisor, for his help, especially in the field and with the images. Further, I thank the SEP (Schweizer Gesellschaft für Schnee, Eis und Permafrost) for the financial enabling of my fieldwork. In addition to the financial contribution, the active support on site was also essential, for which I would like to thank Merit Boomsma. I am also grateful to Pia Biondi, the warden of the Rotondo hut, for her hospitality and the delicious food during the fieldwork, as well as local information, her interest and friendship. I would also like to thank the SLF, or more precisely PERMOS, for making their current confidential database with all recorded events available to me for this work. Additional thanks go to Leah, Chris, and Sonja for critically reviewing this work. Last, but not least, special thanks go to my family and friends for their support throughout my studies and this thesis.

Abstract

Rockfall events pose a danger for people and infrastructure in high mountain areas, expected to intensify with rising temperatures and increased heavy rainfall associated with human-induced climate change. This study applies a new approach, using annual isochrones at the Witenwasserengletscher (UR) as a rockfall archive, to investigate the influence of high temperature and heavy rainfall on rockfall occurrences. Through the analysis of aerial and drone images, a time series of rockfall events was created. Additionally, the size and breakout zone of each event were investigated. A total of 27 events were identified between 1913 and 2014, mainly originating from one part of the headwall consisting of *Zentraler Streifengneis*. The sizes of events varied widely, with volumes ranging from 1 to 561 m³. While no long-term trend in rockfall activity was observed, periods of increased activity correlated with peaks in summer temperatures. However, no direct relationship between extreme rainfall and rockfall events was found. Comparison to the PERMOS database indicated that smaller events were underrepresented there, especially before 2005. The main uncertainties include the identification of isochrones and their allocation to an absolute year. The findings suggest that rockfall events are likely influenced by high temperatures and may consequently increase with rising temperatures in the future.

Table of Contents

Acknowledgments	i
Abstract	ii
List of Figures	v
Figures in the Appendix	vii
List of Tables	ix
Tables in the Appendix	ix
List of Abbreviations	x
1 Introduction	1
1.1 Motivation and Research Gap	1
1.2 Research Questions	3
3 Theoretical Background	4
3.1 Definition and Types of Rockfall	4
3.2 Rockfall Influencing Factors	4
3.2.1 Permafrost Degradation	4
3.2.2 Glacial Retreat – Debuttressing and Stress-Release Fracturing	5
3.2.3 Heavy Rainfall	5
3.3 Development of Isochrones	5
4 Transport of Deposits	6
4.1 Functionality Illustrated with Images	6
5 Study Site	9
6 Methods	11
6.1 GIS Analysis	11
6.1.1 Identification of Deposits and Isochrones	11
6.1.2 Identification of Absolute Time Series	14
6.2 Field Measurements	15
6.3 Analysis of Data	16
6.3.1 Analysis of Collected Data	16
6.3.2 Comparison to Climate Data and Rockfall Database	17
7 Results	20
7.1 Identified Deposit	20
7.2 Interview with Pia Biondi	22
7.3 Identified Events and Time Series	22
7.3.1 Allocation of Absolute Years	22
7.3.2 Properties of Rockfall Events	25
7.3.3 Flow Lines and Geology	29
7.4 PERMOS Database	31

7.5	Climate Variables	34
7.5.1	Mean Summer Temperature	36
7.5.3	Indicator Isochrones	37
7.5.4	Summer Precipitation	38
8	Discussion	39
8.1	Reconstruction of Rockfall Events (Research Question 1.)	39
8.1.1	Frequency and Timing of Rockfall Events (Research Question 1.1)	39
8.1.2	Sizes of Rockfall Events (Research Question 1.2)	40
8.1.3	Geology and Breaking Point of Rockfall Events (Research Question 1.3)	41
8.2	Comparison to PERMOS Database (Research Question 2.)	41
8.3	Comparison to Climate Variables (Research Question 3.)	43
8.3.1	Temperature	43
8.3.2	Rainfall	45
8.4	Outlook	46
9	Conclusion	48
	<i>Literature</i>	49
	<i>Appendix</i>	54
	Figures and Pictures	54
	Tables	63
	<i>Personal Declaration</i>	69

List of Figures

Figure 1: PERMOS rockfall database for the Alps showing the number of events and their volumes over time, including the seasons the events occurred in (PERMOS, n.d.).	2
Figure 2: Sketch of the isochrones and transportation of rockfall deposits (stage 1, 2, 3, 4 and a), b), c)) through a glacier in a steady state.	6
Figure 3: Aerial image of Witenwasserengletscher in 2015 (swisstopo, 2022).	7
Figure 4: a) Snippet of the 2012 aerial image (swisstopo, 2022), b) isochrones of snippet a) with assigned years.	8
Figure 5: Example of rockfall deposits (D1 & D2) that are a) clearly assigned to a year and b) melted out and scattered. a) is from 2008 (swisstopo, 2022); b) is from 2022 (GIUZ, 2022).	8
Figure 6: Localisation of the study area (red mark) a) in Switzerland, b) in the region and c) the immediate surrounding (geo.admin.ch, n.d.).	9
Figure 7: a) Geological map of the Witenwasserren surrounding with legend (b)) (Hafner et al., 1975).	10
Figure 8: Visualisation of the “cross-dating” approach. The categories of the identified deposits are displayed in green, ranging from “with a clear isochrone” (fully saturated) over “with an isochrone, but unsure which one” (less saturated) to “melted out” (least saturated). In case of a second deposit in one year they are displayed in red with the same gradation.	13
Figure 9: Section of the drone image from 2022 with the mapped deposit areas (green; A to V) and zones with additional deposits (orange) (drone image: GIUZ, 2022).	21
Figure 10: Timeline with the number of events per year, where 1 = youngest and 102 = oldest identified isochrone. From left to right the isochrones and events become older.	22
Figure 11: Number of events each year in different scenarios of absolute years, the scenario chosen for subsequent analysis is framed in orange. In the temperature plot the running mean (with $k = 5$) is displayed as a red line, and the mean over the whole period (1907 – 2021) as a dark blue dashed line ($=10.89^{\circ}\text{C}$). The blue dashed vertical lines in the scenarios mark the beginning and end of the isochrone recordings (first and last measured isochrone). (temperature data: MeteoSchweiz, 2023).	24
Figure 12: Properties of the identified events, coloured according to confidence or state of melting out, including legends. The values of the area and volume are rounded to whole numbers, and the years correspond to scenario “images”. The mean thickness corresponds to the mean thickness over the whole deposit. For better visibility, an “R” was added to the “rockfall” class in the block sizes, the smaller circles are “very small” events, and the bigger ones are “blockfalls”. The input data can be found in appendix (Table A. 5).	26

Figure 13: Histograms of the a) block size-based classes (very small < 1 m³, rockfall = blocks < 0.5 m³, blockfall = with blocks > 0.5 m³) and b) event volumes (m³) with equal interval classes. The orange square includes the events which are possibly rockslides. 27

Figure 14: Comparison of the area of the deposits to the mean thickness, including a linear regression. 28

Figure 15: Comparison of the area of the deposits to the mean thickness without the outlier at a thickness of 0.5 m, including a linear regression. 28

Figure 16: Flow lines on the Witenwasserengletscher (dotted lines) created with the MATLAB streamline function based on the DEM from 2019 and the identified geologies (triangles) overlaying the geological map from Hafner et al. (1975). 30

Figure 17: Timeline of the events in the PERMOS database and the events identified at the Witenwasserengletscher (flipped on the x-axis). The beginning of the active database in 2003 is displayed as an orange dashed line (data: PERMOS, 2023). 31

Figure 18: Timeline of the events in the PERMOS database (events with V > 100'000 m³) and at the Witenwasserengletscher (flipped on the x-axis). The beginning of the active database in 2003 is displayed as an orange dashed line (data: PERMOS, 2023). 32

Figure 19: Volumes of the measured deposits and the events in the PERMOS database on a logarithmic scale. The start of the active PERMOS database (vertical) and the volume threshold (horizontal) are marked as an orange dashed line (data: PERMOS, 2023)..... 33

Figure 20: Proportions of the variables a) “glacier” (= glacier in immediate surroundings of rockfall events) and b) “permafrost” (= permafrost occurrence at the events according to Kenner (2018)) in the PERMOS database (n = 459). The category “yes” in subplot a) includes two events with “yes, partially” (data: PERMOS, 2023). 34

Figure 21: PDD, annual mean temperature, mean summer temperature (all three including their mean over the whole period as a blue dashed line and running mean with k = 5 in red), summer ablation of the Claridenfirn (blue), Griesgletscher (green), Grosser Aletschgletscher (orange) and Silvrettagletscher (red), summer precipitation including the total summer precipitation (sum) and the number of days with high amounts of rainfall, and detected rockfall time series from Witenwasserengletscher. The individual climate variables can be viewed in the appendix (Figure A. 4 – Figure A. 8; precipitation and temperature data: MeteoSchweiz, 2023; mass balance data: GLAMOS, 2023)..... 35

Figure 22: Summer temperature, event time series and volumes of the events over time, with the running means in red (temperature k = 5 a; events k = 3 a) and the mean of the temperature from 1910 to 2017 (=10.85°C) in dark blue and dashed. The volumes of two events in one year are

cumulated, and the volumes of the second deposits are displayed in orange. For better visibility, the smallest volumes are circled in light blue (temperature data: MeteoSchweiz, 2023).	36
Figure 23: Timeline with the identified indicator isochrones and the years with deposits.	37
Figure 24: Proportions of the indicator years, rockfall event years, and indicator years with events, a) as identified and b) including the indicator years one year before or after an event (n = 2) in the category combining the two variables (total = 102 years).	37
Figure 25: Number of days with extreme precipitation in the summer months (June, July, August) in Andermatt and the detected event timeline (flipped on the x-axis) (precipitation data: MeteoSchweiz, 2023).....	38
Figure 26: Cutout of the drone image from 2022 with deposits A25, A26 and A27 (GIUZ, 2022).	40
Figure 27: Allocation of the periods with increased rockfall activity to peaks in summer temperature (“wiggle matching”; in green and violet) including the mean of the summer temperature per year (in black), event time series, and volumes of the events over time. With the running means in red (temperature k = 5 a; events k = 3 a) and the mean summer temperature over the whole period (=10.81°C) as a dark blue dashed line. The volumes of two events in one year are cumulated, the volumes of the second deposits are displayed in orange (temperature data: MeteoSchweiz, 2023). .	44

Figures in the Appendix

Figure A. 1: Permafrost distribution in the surrounding of the Witenwasserengletscher according to Kenner (2018) (background map: Swisstopo, n.d.).	54
Figure A. 2: Permafrost distribution in the surrounding of the Witenwasserengletscher according to Swisstopo (BAFU, 2005; background map: Swisstopo, n.d.).	54
Figure A. 3: Pictures of the squares investigated in the field which were allocated to a deposit in the GIS, including the deposit name and measurement name.	55
Figure A. 4: Annual mean temperature at the station in Andermatt from 1913 to 2014 with a mean over the displayed period (= 7.42 °C; blue dashed line) and a running mean (red) with k = 5 a (data: MeteoSchweiz, 2023).	59
Figure A. 5: Mean summer temperature at the station in Andermatt from 1913 to 2014 with a mean over the displayed period (= 10.81 °C; blue dashed line) and a running mean (red) with k = 5 a (data: MeteoSchweiz, 2023).	60
Figure A. 6: Positive degree day at an elevation of 3000 m a.s.l.(lapse rate = 0.6 °C per 100 m) with a mean over the displayed period (= 1742.16 °C; blue dashed line) and a running mean (red) with k = 5 a (data: MeteoSchweiz, 2023).	60

Figure A. 7: Summer precipitation in Andermatt from 1913 to 2014. Sum of summer precipitation (mm) and number of days with particularly large amounts of rain (data: MeteoSchweiz, 2023). 61

Figure A. 8: Summer mass balance of the Claridenfirn, Griesgletscher, Silvrettagletscher and Grosser Aletschgletscher, each with the mean value (dashed lines) from the beginning of their measurement to 2014 (data: GLAMOS, 2023)..... 61

Figure A. 9: Residual diagram of the linear regression of the area and thickness. 62

Figure A. 10: Residual diagram of the linear regression of the area and thickness without the outlier with a thickness of 0.5 m..... 62

List of Tables

Table 1: Metadata of the images used for the analysis.	11
Table 2: Different scenarios of the absolute timeline and how they were determined.....	14
Table 3: Metadata of the external datasets.....	17
Table 4: Information about the four glaciers included in the mass balance series.	18
Table 5: Number of identified deposits in each image and number of deposits assigned to an isochrone.	21

Tables in the Appendix

Table A. 1: Notes and remarks during the identification of the deposits on the Witenwasserengletscher on the drone image from 2022 (GIUZ, 2022).	63
Table A. 2: Data acquired in the field and allocation of measurements to deposits identified in GIS (AX).	64
Table A. 3: Notes from the interview with Pia Biondi (warden of the Rotondo hut) on 23.08.2023. ...	67
Table A. 4: Contacts and archives for the search of historical photographs.	67
Table A. 5: Measured and calculated variables of the identified rockfall deposits. “Melted out” refers to the deposit being melted out at the time of the area measurement (1 = yes, 0 = no), the thickness is the mean thickness in the covered part. “Confidence” refers to the confidence of the thickness and percentage coverage (0 = freely estimated (low confidence), 1 = similar to measurement, 2 = measured (high confidence)). “Block” refers to the block size-based classification (1 = “very small”, 2 = “rockfall”, 3 = “blockfall”) and the “confidence block” refers to the confidence these classes. The last three columns show the number of images the deposits are “with an isochrone”, “melted out” and “with an isochrone, but unsure which one” respectively.....	68

List of Abbreviations

a.s.l.	Above sea level
BGS	Bodenkundliche Gesellschaft der Schweiz
ELA	Equilibrium Line Altitude (border between accumulation and ablation area)
GIS	Geographic Information System
GIUZ	Department of Geography (University of Zurich)
GLAMOS	Glacier Monitoring Switzerland
GPR	Ground Penetrating Radar
GPS	Global Positioning System
IPCC	Intergovernmental Panel on Climate Change
PDD	Positive Degree Day Sum
PERMOS	Swiss Permafrost Monitoring Network
SAC	Swiss Alpine Club
SLF	WSL Institute for Snow and Avalanche Research (WSL = Swiss Federal Institute for Forest, Snow and Landscape Research)

1 Introduction

1.1 Motivation and Research Gap

Rockfall events are a hazard to human infrastructure and activities in high mountain areas and can even end deadly (e.g. Dikau and Glade, 2002; Allen and Huggel, 2013; Deline et al., 2015; Haeberli and Whiteman, 2015). With the expansion of activities and infrastructure to mountainous regions the risk increases and the understanding of rockfall processes becomes increasingly important (Haeberli & Whiteman, 2015). Furthermore, rockfalls can trigger cascading events such as snow avalanches (Haeberli & Whiteman, 2015), the building of new lakes (Deline et al., 2015; Evans & Delaney, 2015), and glacial lake outburst floods (GLOFs) (Carey et al., 2021).

Past studies of individual documented rockfall events have compared the events and established favouring factors of such events. These include factors with causes in geology, climate, soil, vegetation, hydrology, and topography, as well as anthropogenic causes (Dikau & Glade, 2002). The climatic factors include high temperatures (e.g. Allen & Huggel, 2013; Gruber et al., 2004; Gruber & Haeberli, 2007; Noetzli et al., 2003; Ravelin et al., 2017; Ravelin & Deline, 2010; Street et al., 1990) and heavy rainfall (e.g. Allen & Huggel, 2013; Wiczorek & Jäger, 1996). With human-induced climate change, these factors are expected to increase (IPCC, 2007; Noetzli et al., 2003; Ravelin & Deline, 2010; Street et al., 1990), which enhances the importance of their understanding. The assumed connection of rising temperatures and heavy rainfall to the rockfall occurrence is however not well constrained by empirical data.

The Swiss Permafrost Monitoring Network (PERMOS) provides a rockfall database for the Alps (Figure 1). The database was created in the heatwave summer of 2003 and has been fed with information on current rockfall events by the public ever since. The events prior to 2003 were compiled from reports. Since the database is fed by reporting it is subject to a bias due to rising awareness, increased access to smartphones, more people in the mountains and other aspects, leading to the incompleteness of the dataset (PERMOS, n.d.; Phillips, 2024a).

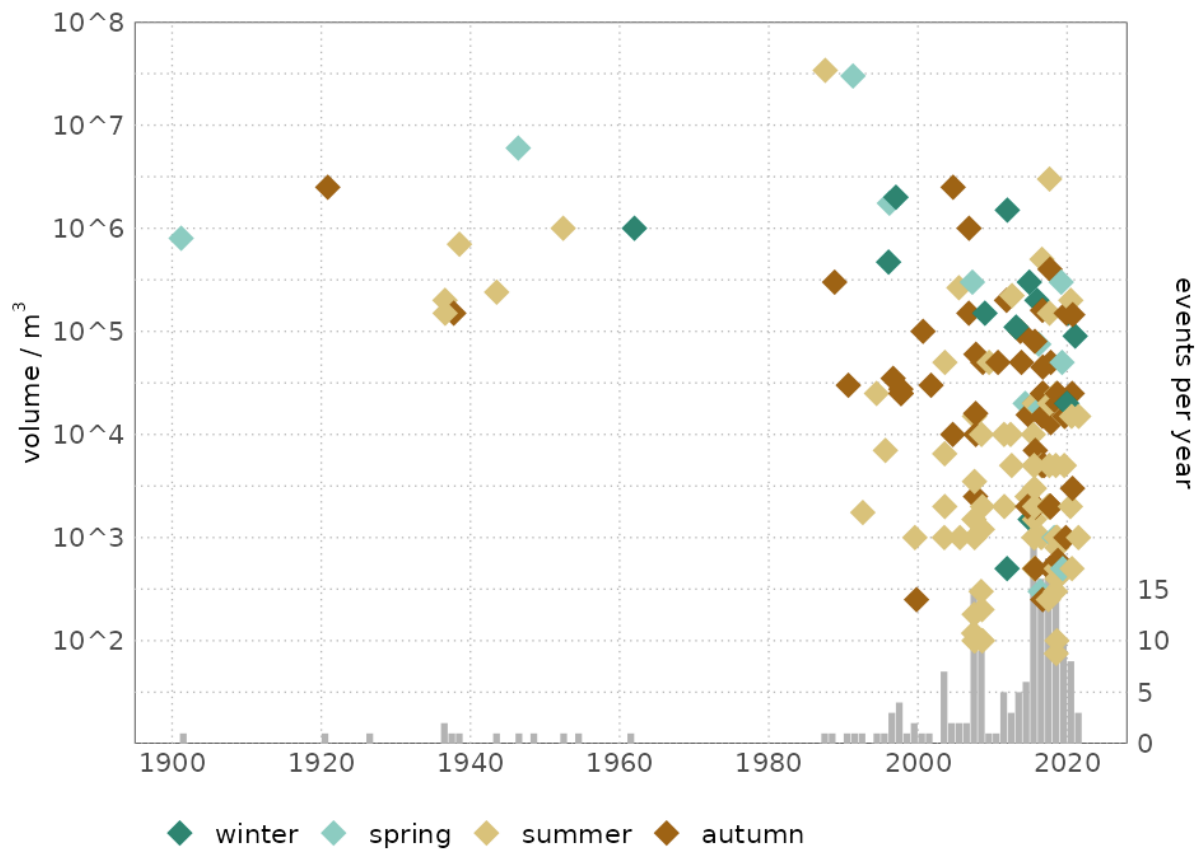


Figure 1: PERMOS rockfall database for the Alps showing the number of events and their volumes over time, including the seasons the events occurred in (PERMOS, n.d.).

This study examines the relationship of rockfall occurrences to rising temperatures and heavy rainfall through an empirical approach. Thereby, a rockfall time series will be reconstructed based on rockfall deposits connected to isochrones visible on a glacier's surface. Since these requirements are met at the Witenwasserengletscher, it is used as the basis for the investigation.

By reconstructing rockfall events at one location over time, other factors influencing slope stability such as soil properties, slope exposure, rock types, and slope inclination remain largely unchanged. Additionally, the observation bias can be avoided with the applied approach. Thus, from such time series, correlations with climate factors, as hypothesised by previous studies (e.g. Allen & Huggel, 2013; Gruber et al., 2004; Gruber & Haeberli, 2007; Noetzli et al., 2003; Ravanel et al., 2017; Ravanel & Deline, 2010; Street et al., 1990; Wieczorek & Jäger, 1996), can presumably be better extracted.

1.2 Research Questions

To examine the suggested relationship between rockfall occurrence and climate factors, a new approach to reconstruct rockfall events will be applied to the Witenwasserengletscher. The following questions are thereby specifically addressed.

1. Can rockfall events in the catchment area of the Witenwasserengletscher (UR) be reconstructed from deposits on the glacier?
 - 1.1 When and how frequently did such rockfall events occur?
 - 1.2 How big were these events?
 - 1.3 What are the transport routes and geology of the deposits, and can they be used to reconstruct the breakout zone?
2. How do the rockfall events at Witenwasserengletscher correlate with periods of increased events elsewhere in the Alps as recorded in the PERMOS database?
3. Is there a connection between the rockfall event frequency on the Witenwasserengletscher and climate factors, specifically temperature and rainfall levels?

3 Theoretical Background

3.1 Definition and Types of Rockfall

Luckman (2013, p. 174) defines rockfall as “the free or bounding fall of rock debris down steep slopes under the influence of gravity”. Volumes of several million cubic meters or just single boulders can thereby be detached from the rock wall (Alberti & Spreafico, 2019). Rockfall events can be divided into two categories based on the diameter of single blocks. Events with single blocks diameters below 50 cm are described as “rockfall”, while events with block diameters above 50 cm are defined as “blockfall” (SLF, n.d.). Additionally, if the events reach a total volume of over 100 m³, they can be described as “rockslides” (PLANAT, n.d.; SLF, n.d.). According to SLF (n.d.) this is the only crucial characteristic of a rockslide. PLANAT (n.d.) however states that in rockslides, in contrast to rockfalls and blockfalls, a large mass of rock detaches from the rock face in one piece and breaks up into individual chunks during the fall or on impact. In this work, rockfall will be used as an overarching term for all events, no matter the block size and total volume, consistent with the current literature.

3.2 Rockfall Influencing Factors

The stability of a rock wall is influenced by several different factors and varies over time (Alberti & Spreafico, 2019). The factors can be divided into preparatory and triggering factors. The main predatory factors include geological discontinuities and weathering, the topography (exposure and slope height), the surface cover (e.g. vegetation) and the ice conditions (glaciers and permafrost) (Deline et al., 2015; Dikau & Glade, 2002; Ohmura, 2015). As the cryosphere is strongly linked to climatic conditions and therefore influenced by the ongoing human-induced global warming (IPCC, 2013), ice conditions are currently influencing the occurrence of rockfall events in particular (Deline et al., 2015). The triggering factors include for example earthquakes and heavy precipitation events (Dikau & Glade, 2002).

3.2.1 Permafrost Degradation

Permafrost refers to soil and rock that have been continuously frozen, with temperatures consistently below 0°C for a duration of two years or more (Dobinski, 2011). The uppermost part, called the active layer, thaws every summer and freezes again in the fall (Gervais, 2015). With higher temperature, this layer becomes thicker (Allen & Huggel, 2013; Street et al., 1990; Streletskiy et al., 2015). Therefore, rising temperature due to climate change favours rockfall events through permafrost thawing, leading to increasingly greater terrain instability (e.g. Allen & Huggel, 2013; Gruber et al., 2004; Gruber & Haeberli, 2007; Noetzli et al., 2003; Raveland & Deline, 2010; Street et al., 1990; Streletskiy et al., 2015). The climate-driven degradation of permafrost is therefore an important mechanism when looking at the climate’s influence on slope stability and rockfall events (Gruber & Haeberli, 2007).

3.2.2 Glacial Retreat – Debuttressing and Stress-Release Fracturing

Studies show that a large proportion (20 – 25%) of rockfall events occur from rock walls above or directly adjacent to a glacier (Deline et al., 2015; Evans & Delaney, 2015). There are two main processes through which the retreat and thinning of glaciers influence slope stability: glacial debuttressing (e.g. Ballantyne, 2002; Haerberli et al., 2013; McColl, 2012) and stress-release fracturing through crustal rebound (Deline et al., 2015; McColl, 2012). Glacial debuttressing describes the loss of slope support provided by glacial ice, which can lead to immediate or delayed rock slope failure (Deline et al., 2015). The relief of glacial ice can further cause a rebound of crustal material which can lead to fractures in the rocks parallel to the surface. These fractures generate potential breaking points for rockfalls (Deline et al., 2015). Additionally, through the retreat and thinning of the glacier new land is exposed (Bolch & Christiansen, 2015; Deline et al., 2015) leading to more material being available for rockfall.

3.2.3 Heavy Rainfall

Heavy rainfall is postulated to exert a favourable influence on the occurrence of rockfall events (Dikau & Glade, 2002; v. Elverfeldt et al., 2008) through rising cleft and pore-water pressure caused by water infiltration (Allen & Huggel, 2013; Wieczorek & Jäger, 1996). Allen & Huggel (2013) observed rainfall of up to 100 mm in the week prior to rockfall events, possibly influencing them. It is expected that heavy rainfall increases due to climate change (IPCC, 2007).

3.3 Development of Isochrones

Cogley et al. (2011, p. 56) define isochrones in the context of glaciers as “a surface that formed at the same time over its entire extent”. They represent former surfaces of an ice sheet or glacier (Hammer, 1980 in Nereson et al., 1998; Hindmarsh et al., 2009) and are traces of firn layers in the accumulation area caused by the alternation of periods with high and low precipitation (Internationale Gletscherconferenz von 1899 in Hess, 1902). During periods with low precipitation, the upper layer of the firn starts to melt and is enriched with weathering dust, leading to a dark coloration of the layer. This layer is in turn covered by snow, which leads to a layering of alternating light and dark stripes (Internationale Gletscherconferenz von 1899 in Hess, 1902), correlating to annual cycles of low (summer) and high (winter) precipitation in the form of snow. On a glacier in the steady state, the isochrone from the previous year (summer layer) corresponds to the ELA (Equilibrium Line Altitude) and their age increases when moving down the glacier (see Figure 2). Isochrones are not to be confused with ogives, which originate from the glacier passing an ice fall (Post & Lachapelle, 2000). They show similar patterns on the glacier surface, but in contrast to isochrones, ogives are only a phenomenon on the surface and do not extend through the entire glacier.

4 Transport of Deposits

Debris that is deposited on a glacier's surface can be entrained and transported by the glacier (Bennett & Glasser, 2009). Figure 2 shows the transport routes of the rockfall deposits through a glacier in a steady state. The isochrones develop in the accumulation area of the glacier and are then transported downwards. Below the ELA they are melted out and become visible on the surface of the glacier. The rockfall deposits from the headwall are deposited in the accumulation area of the glacier (1). They are then transported through the glacier on the isochrone they were deposited on (2). As they are transported downwards (a), they are also transported forward with the glacier flow (b). At some point, they melt out to the glacier's surface with a clear edge at the isochrone (3). From there the rockfall deposits are further transported on the glacier surface (c), melting out further and being scattered. As soon as the whole deposit is melted out, it is disconnected from the isochrone (4) (Benn & Evans, 2010; Bennett & Glasser, 2009; Goodsell et al., 2005).

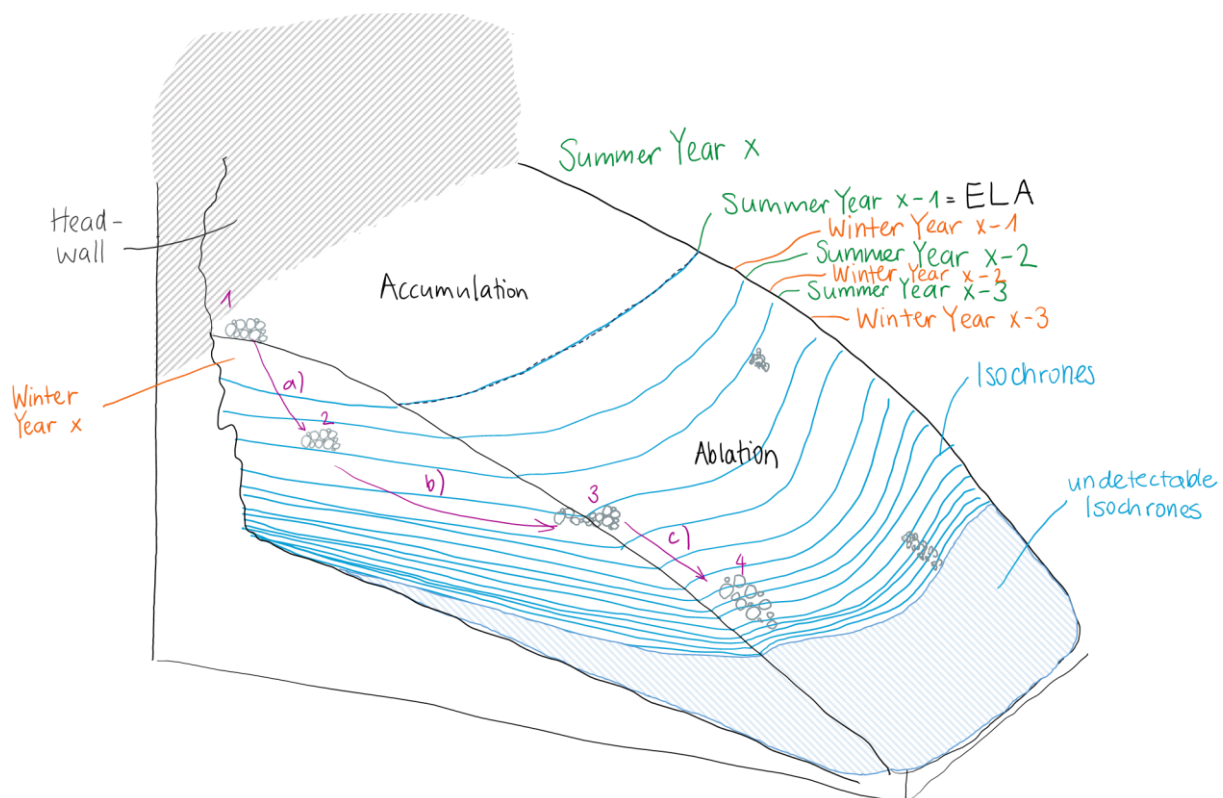


Figure 2: Sketch of the isochrones and transportation of rockfall deposits (stage 1, 2, 3, 4 and a), b), c)) through a glacier in a steady state.

4.1 Functionality Illustrated with Images

Figure 3 shows the view on the Witenwasserengletscher from above, revealing isochrones and deposits. The zoom-in (Figure 4) displays how the isochrones are assigned to a year and Figure 5 demonstrates the process of the deposits melting out and being scattered over time.

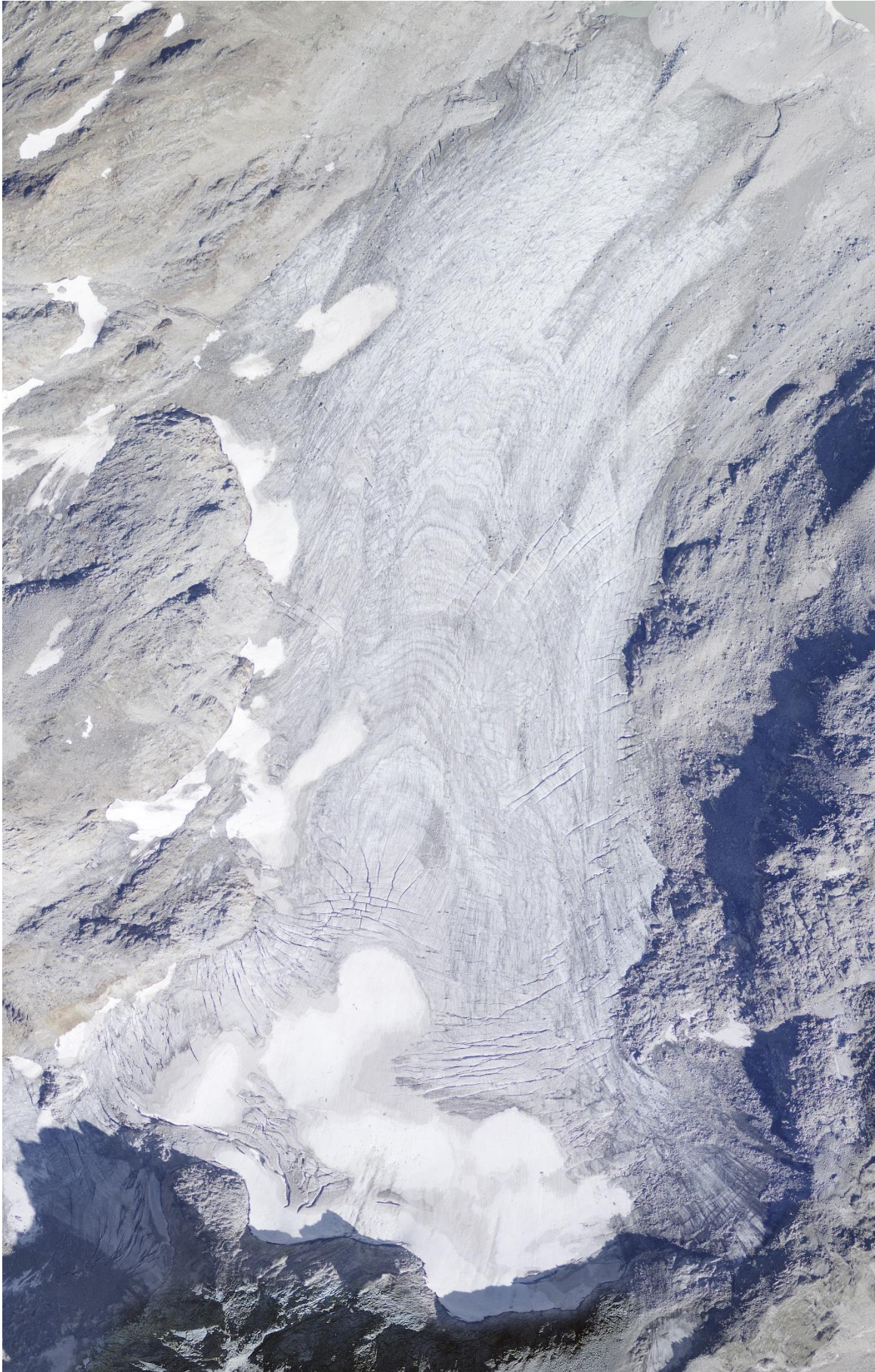


Figure 3: Aerial image of Witenwasserengletscher in 2015 (swisstopo, 2022).

a)



b)

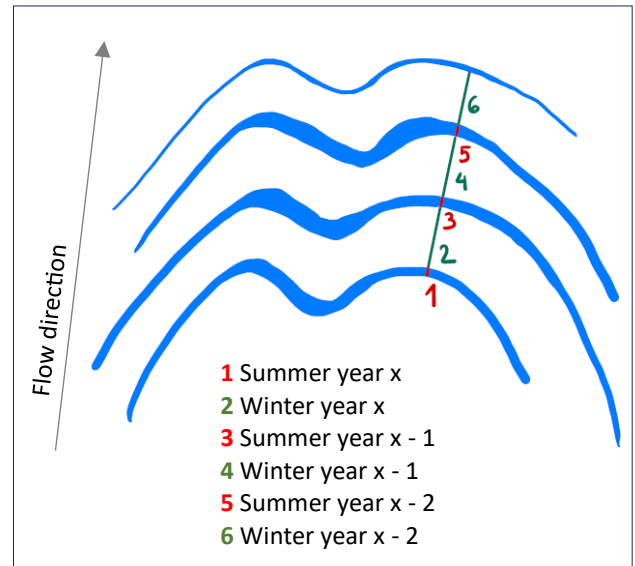
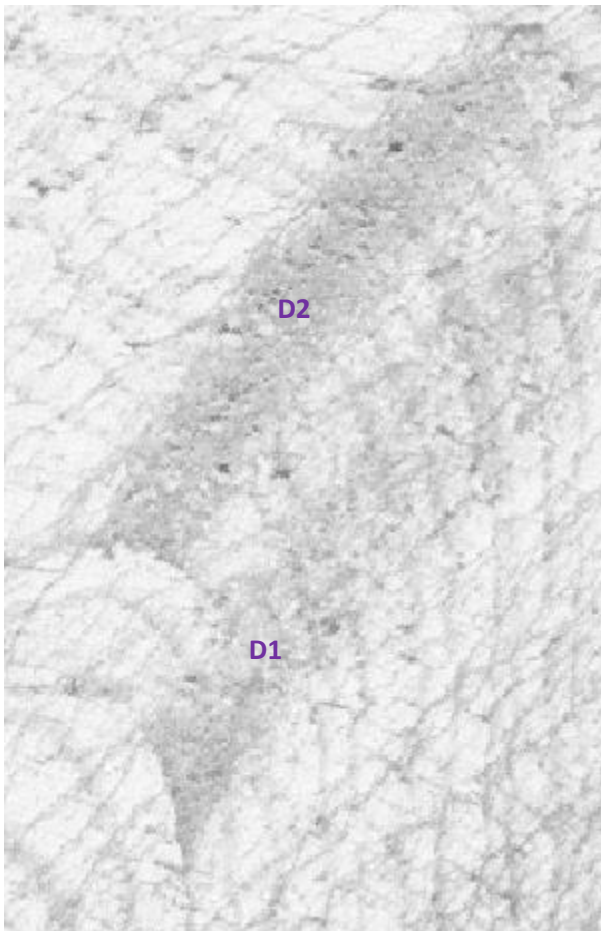


Figure 4: a) Snippet of the 2012 aerial image (swisstopo, 2022), b) isochrones of snippet a) with assigned years.

a)



b)

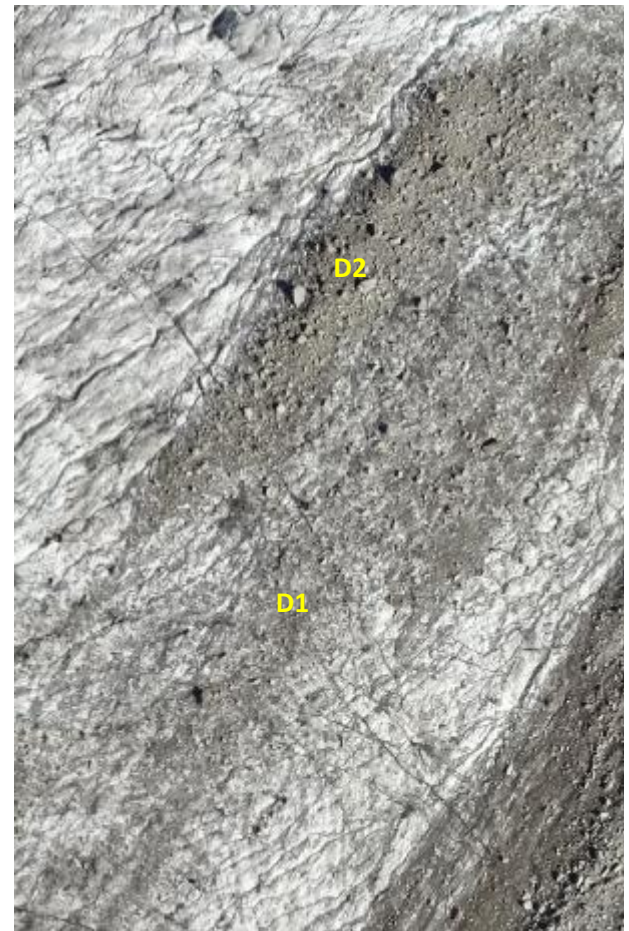


Figure 5: Example of rockfall deposits (D1 & D2) that are a) clearly assigned to a year and b) melted out and scattered. a) is from 2008 (swisstopo, 2022); b) is from 2022 (GIUZ, 2022).

5 Study Site

The Witenwasserengletscher is located within the Swiss Alps in the Gotthard region close to the town of Andermatt in the canton of Uri (see Figure 6 a) & b)). It is north-exposed and has a headwall shading it to the south (Figure 6 c)). The glacier extends from 2545 to 2900 meters above sea level (m a.s.l.), while its headwall rises from 2900 to 3085 m a.s.l. (swisstopo, n.d.). According to models from Kenner (2018; Figure A. 1) and Swisstopo (BAFU, 2005; Figure A. 2) the presumed release areas (= origine of the rockfalls) above the Witenwasserengletscher consist of permafrost.

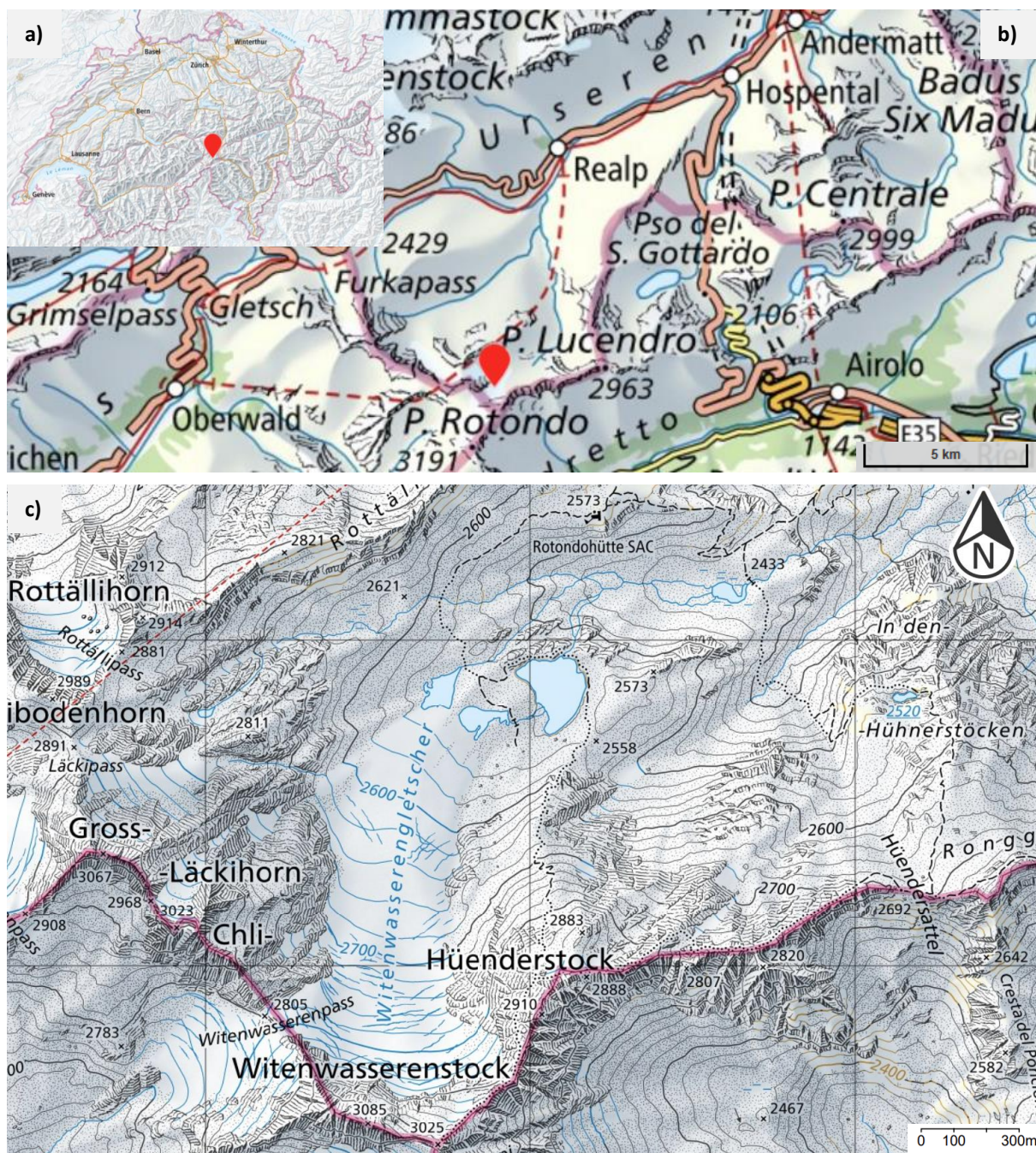
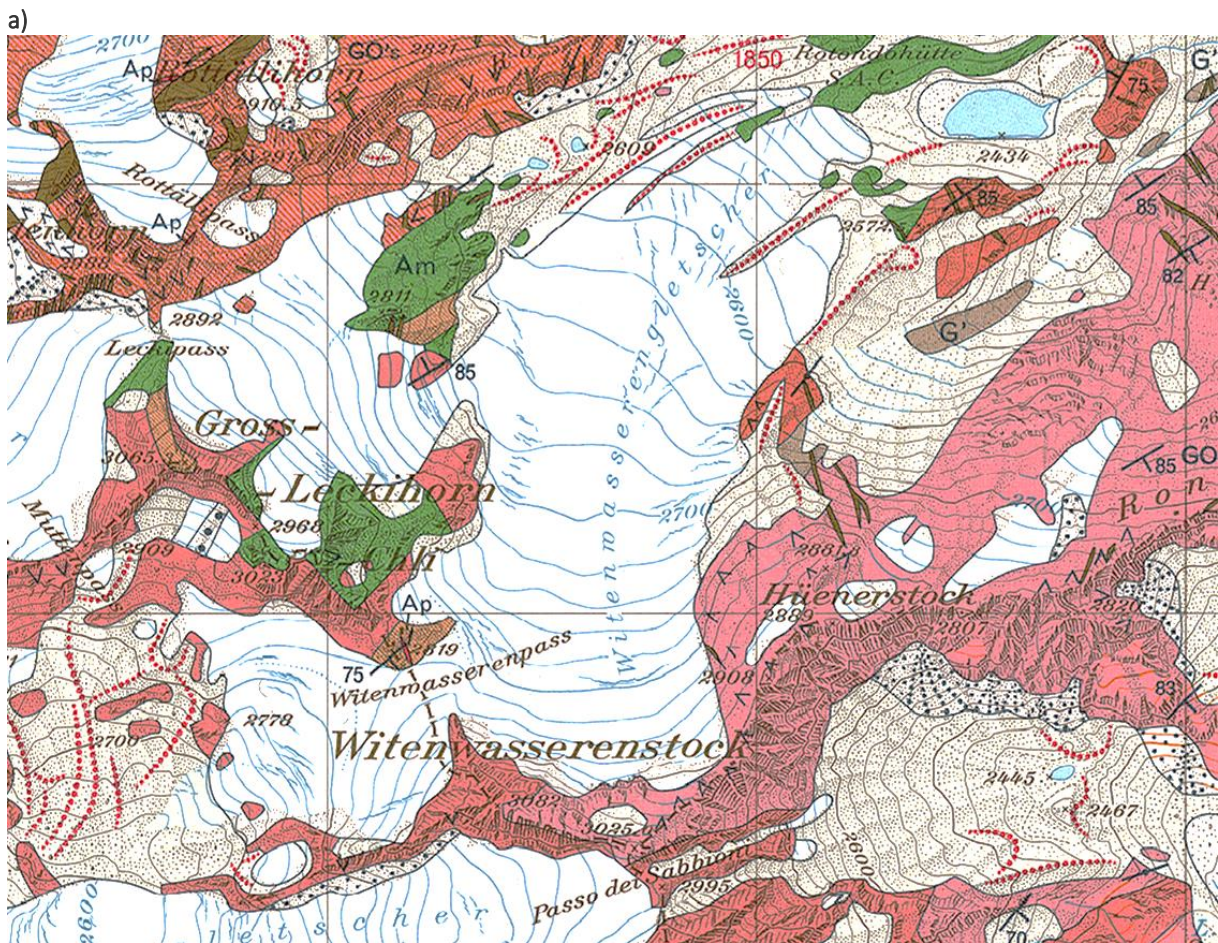


Figure 6: Localisation of the study area (red mark) a) in Switzerland, b) in the region and c) the immediate surrounding (geo.admin.ch, n.d.).

The geology around the Witenwassere ngletscher belongs to the Gotthard massif and is largely made up of *Zentraler Streifengneis* (engl. from legend: strained gneiss, light mica-alkali feldspar gneiss) and *Rotondogranit* (engl. from legend: massive aplite granite, even-grained, biotite-bearing) (Figure 7).



b)

Objekt	
Heller Glimmer-Alkalifeldspatgneis (Zentraler Streifengneis)	
Massiger Aplitgranit, gleichkörnig, biotitführend (Rotondogranit)	
Feinflaseriger Biotit-Plagioklasgneis, oft mit biotitreichen Schmitzen (Oberstafel-Gneis)	
Amphibolite, Hornblendeschiefer und-gneise, oft wechsellagernd mit hornblendefreien Glimmergneisen (Bänderamphibolite)	
Helle, feinstreifige Glimmer-Alkalifeldspatgneise, Glimmer-Plagioklasgneise und-schiefer, aplitische Lagen, pegmatitische Gänge und Linsen (Prato-Serie u.a.)	
Dunkle Biotit-Sericitgneise und-schiefer (Giubine-Serie u.a.)	
Rezente & subrezente Moräne, Moränenwall (red dots)	

Figure 7: a) Geological map of the Witenwasseren surrounding with legend (b)) (Hafner et al., 1975).

6 Methods

The goal of this study is to develop a time series of rockfall events from the Witenwasserengletscher's headwall. To do so, the isochrones and deposits on the glacier were investigated with different methods including GIS analysis, field work, and data analysis.

6.1 GIS Analysis

The GIS (geographic information system) analysis was executed in Version 3.28 *Firenze* of the open-source software *QGIS*. Five aerial images from *Swisstopo* and two drone images collected by the Department of Geography, University of Zurich, were studied (Table 1). The drone images were collected with an *eBee X* drone equipped with a *Sony WX RGB* optical camera. All images were recorded in summer, when a large part of the glacier was not covered with snow.

Table 1: Metadata of the images used for the analysis.

Image	Source	Type	Resolution	Colour	Date
2023¹	GIUZ (2023)	Drone image	0.1m	RGB	23.08.2023
2022	GIUZ (2022)	Drone image	0.1m	RGB	22.08.2022
2015	swisstopo (2022)	Aerial image	0.25m	RGB	unknown
2012	swisstopo (2022)	Aerial image	0.25m	RGB	unknown
2008	swisstopo (2022)	Aerial image	0.5m	Black & white	29.08.2008
2003	swisstopo (2022)	Aerial image	0.25m	RGB	17.09.2003
2000	swisstopo (2022)	Aerial image	0.5m	Black & white	25.08.2000

¹This image was just used for part of the analysis as it became available only at a later stage of this research

6.1.1 Identification of Deposits and Isochrones

In a first step, all deposits were identified in the drone image from 2022 to get a first impression of their distribution. Simultaneously, it was determined whether they had a clear edge at an isochrone. Moreover, the areas of the deposits were measured with the *field calculator* (function $\$area$) and some additional observations were listed (Table A. 1).

In a second step, the isochrones were identified on each image. They were counted from the top of the glacier to the bottom and given a number, with different numbers for each image. In the same step, the isochrones were classified into visibility classes. The classes were defined as (I) quasi nonvisible/very insecure, (II) visible, but not very good/quite secure and (III) very good visible/secure. Additionally, each isochrone was characterised as an isochrone with or without deposition. Further, the number of deposits and how many of them were connected to an isochrone was determined for each image.

After each image was analysed individually, a “cross-dating” approach was performed between the images in a third step (Figure 8). Each deposit was thereby assigned to one of the categories “with a clear isochrone”, “with an isochrone, but unsure which one” or “melted out” in each image (cf. Figure 5). The analysis was continued only with the deposits connected to an isochrone in at least one image. Next, the assumed number of isochrones between the deposits in each image was compared. As they varied between the pictures, the correct number of years had to be investigated. With the help of the assigned visibility classes and visual validation, one timeline with the counted number of years and deposits was created.

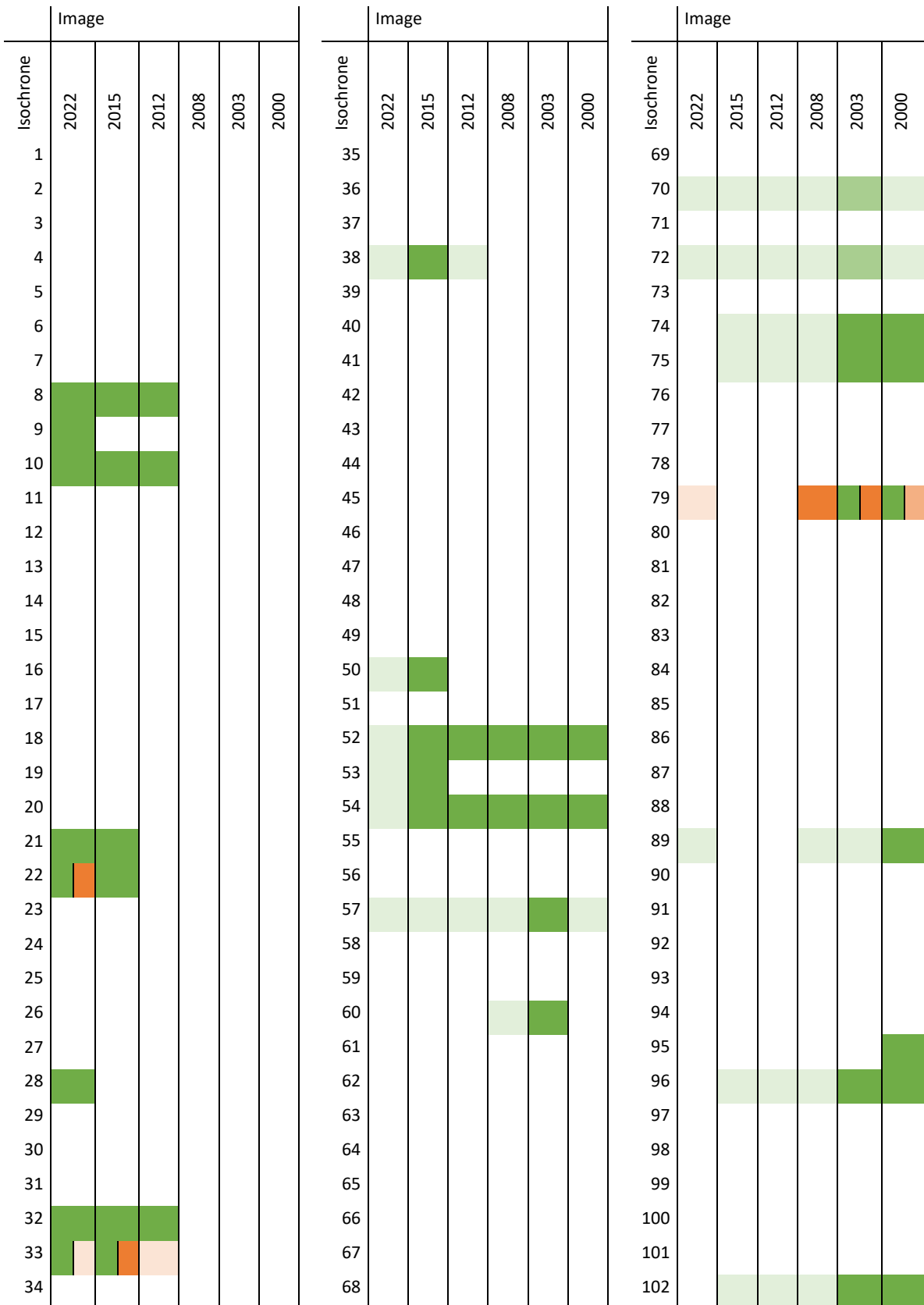


Figure 8: Visualisation of the “cross-dating” approach. The categories of the identified deposits are displayed in green, ranging from “with a clear isochrone” (fully saturated) over “with an isochrone, but unsure which one” (less saturated) to “melted out” (least saturated). In case of a second deposit in one year they are displayed in red with the same gradation.

Subsequently, the areas of the determined deposits were estimated. For this, the image in which the deposits were melted out the most, but still clearly visible (not scattered) was chosen. This was not always the newest image they were in, but as new as possible while still being able to measure clearly. To assess whether the measured areas corresponded to the entire deposit, it was also determined whether the deposit was melted out in the image where the area measurement was taken. When the deposit is not fully melted out yet, the area (and later the volume) is most likely underestimated as part of the event still remains in the glacier (cf. Figure 2 & Figure 5). It is therefore assumed that volumes calculated based on areas from completely melted out deposits correspond better to the actual volume of the events. The outlines of the deposits, which were determined by visual delineation, served as the basis for the area calculations with the *\$area* function in the *field calculator*. Some deposits were split up into several areas due to varying densities and thicknesses within the deposit, based on visual aspects in the images and field observations (cf. 6.2). These measurements could only be conducted in the two drone images from 2022 and 2023, due to insufficient spatial resolution of the aerial images. Furthermore, crevasses were counted as part of the areas since they also contain rocks.

6.1.2 Identification of Absolute Time Series

To determine the absolute years of the developed timeline, four scenarios were investigated (Table 2). Two of them (2022 & “images”) were determined by counting isochrones in different images, where the topmost (= youngest) visible isochrone always corresponds to the previous year or earlier (see Figure 2). Scenarios 2003 and 1994 were identified through the allocation of peaks in summer temperature to isochrones. Two properties of the isochrones influenced by high temperature were considered for this purpose. With more ablation (and less accumulation) isochrones become narrower and a higher melting rate increases the intrusion of fine material into the summer layer leading to particularly dirty isochrones (Hess, 1902). Therefore, particularly narrow or dirty isochrones were used as indicators for exceptionally warm (summer) temperatures. These indicator isochrones were also used for additional analysis (cf. 6.3.2). Finally, the most realistic scenario was determined for subsequent analysis.

Table 2: Different scenarios of the absolute timeline and how they were determined.

Scenario	Description
2022	In the drone image from 2022 the topmost isochrone was set as 2021.
“images”	In each image the topmost isochrone was set to one year before the image was taken.
2003	The topmost indicator isochrone was set as the extremely warm year 2003.
1994	The topmost indicator isochrone was set as the extremely warm year 1994.

As another approach to determine an absolute year in the timeline, aerial images and historical photographs from the area were investigated, looking for a fresh deposit. A fresh deposit in an image would have been clearly datable and could have been identified again in the ablation area and thus serve as a reference point for absolute dating. Several different sources were contacted for this purpose, namely aerial images (swisstopo, 2022), the ETH photo archive (Swisscovery, n.d.), the warden of the Rotondo hut, SAC Lägern (the owner of the hut), the municipality of Realp and the Talmuseum Urseren.

6.2 Field Measurements

In addition to the GIS analysis, some data was collected in the field between 21.08.2023 and 24.08.2023. The identified depositions in the drone image from 2022 built the foundation for the field work, defining possible measurement points distributed across the glacier. For some deposits, more than one point was determined due to the different thicknesses and densities within the deposit (cf. 6.1.1 & Figure A. 3).

In total, 38 sites were sampled, with several different measurements at each site. On every site a square of two-by-two meters was fixed, sketched, and photographed (Figure A. 3). With a *Garmin eTrex 10* handheld GPS, the coordinates of the square centres as well as the elevation were measured, with some inaccuracies due to different measuring times and signal problems. Additionally, the rock types were determined for each deposit based on the descriptions of Meyer (2022). Further, for each square, the percentage of rock coverage was determined visually with the help of the “Vergleichstafel zur Skelettschätzung” (BGS, 2010) usually used to determine the skeleton content in soils. Next, the percentages of different grain, rock and block sizes were identified (as percentages of the covered part). The rocks were divided into seven categories: < 5 cm, 5 – 10 cm, 10 – 20 cm, 20 – 30 cm, 30 – 50 cm, 0.5 – 1 m and > 1 m. The first couple of measurements were conducted with different categories, which were then revised and reallocated to the categories defined above in post-processing. Furthermore, the mean thickness of the different categories was estimated, and some additional remarks were made. These included for example information on the presence of sand and notes about the topography of the deposits (e.g. elevation due to reduced melt). All notes from the field are listed in Table A. 2 in the appendix. Additionally, a short interview with Pia Biondi was conducted (Table A. 3), who has been the warden of the Rotondo hut since 2015, which is situated with a good view of the Witenwasserengletscher (cf. Figure 6 c)).

6.3 Analysis of Data

6.3.1 Analysis of Collected Data

The data collected in the field and in GIS was later analysed. First, the data collected in the field was processed and unified. Second, the measurements were allocated to the deposits identified in the GIS analysis (cf. Table A. 2). Calculations were done to add further variables to the analysis, most importantly the mean measured thickness in the covered part (= h_{CP}) as well as the mean thickness over the whole area (= h_A). The mean measured thickness in the covered part was defined by a combination of the estimated percentages per size category and mean thickness per category. The mean thickness over the whole area was then calculated using equation (Eq. 1).

$$h_A [m] = h_{CP} [m] \times coverage [\%] \quad (\text{Eq. 1})$$

By multiplying h_A with the area measurements from the GIS analysis, the volume of each event was calculated. Additionally, the events were categorized into “very small”, rockfall, and blockfall according to the block sizes determined in the field or from the drone image (including the confidence classes “measured in field”, “measured in image”, and “estimated”). The events were also categorized as rockslide depending on their total volume.

For some events, the thickness and percentage coverage were estimated from the aerial images as they were not determined in the field due to safety reasons, or because the deposits were not on the glacier anymore. This was done through visual comparison of these deposits in the aerial images to similar looking ones in the drone images, which were measured in the field. For very thin deposits where no comparable measurements were available, the thickness and percentage coverage were visually approximated from the aerial images. Due to these uncertainties, confidence classes for the thickness and percentage coverage were added with 0 = freely estimated (low confidence), 1 = similar to measurement, and 2 = measured (high confidence).

The relationship between the area of the deposits and their mean thickness over the whole area was also investigated. Thereby, it was tested statistically whether the thickness increases linearly with increasing area. This was done with a linear regression model, revealing more about the relationship between the area and volume of a deposit and whether the volume could be derived directly from the area measurements without including thickness values.

Further, a histogram of the volumes was generated with five classes defined by the equal interval function (Eq. 2). With this method, all intervals have the same size, which is helpful to see the distribution of the values.

$$\text{Intervall Size} = \frac{\text{max Value} - \text{min Value}}{\text{Number of Intervals}} \quad (\text{Eq. 2})$$

To determine the breakout zone of the rockfall events, a flow path analysis was done. The flow routes were generated with the *MATLAB streamline* function based on the surface gradient field from the swissALTI3D DEM (swisstopo, 2018). Thereby, imaginary deposits were planted at 29 points at the foot of the headwall. This was later combined with the geology measured in the field.

6.3.2 Comparison to Climate Data and Rockfall Database

To investigate the relationship between the collected data and climate variables as well as the already existing rockfall database from PERMOS, variables from external datasets (Table 3) were analysed and compared to measured variables. The temperature and precipitation data were collected at the meteorological station in Andermatt (ANT) at 46.630914N / 8.580553W at an altitude of 1435 m a.s.l.

Table 3: Metadata of the external datasets.

Data	Temporal Resolution	Spatial Expansion	Source
Temperature	Monthly ¹ & daily ²	1 Station (Andermatt)	MeteoSchweiz (2023)
Precipitation	Monthly	1 Station (Andermatt)	MeteoSchweiz (2023)
Mass balances	Seasonal	4 Glaciers in Swiss Alps	GLAMOS (2023)
Rockfall series	-	Alps (mainly Switzerland)	PERMOS (2023)

¹Monthly temperature data was used for the annual mean and summer mean.

²Daily temperature data was used for the PDD.

Temperature

For the temperature analysis, the annual mean (Figure A. 4), the mean summer (June, July, August) temperature (Figure A. 5), and the positive degree day sum (PDD) (Figure A. 6) were determined. The summer temperature was included because it is expected to have a greater influence on permafrost thawing and the melt of the glacier than the annual mean values. To incorporate extremely warm days into the analysis, the PDD was determined. For this, the temperature at a height of 3000 m a.s.l., this corresponds to the approximate mean height of the glacier's headwall (swisstopo, n.d.), had to be calculated first. The temperature was derived from the measured temperature at the meteorological station in Andermatt (1435 m a.s.l.) using a lapse rate of -0.6 °C per 100 m elevation rise, which

corresponds to a normal dry adiabatic gradient (Fairbridge & Oliver, 2005). The PDD for each year was then determined with equation (Eq. 3).

$$PDD [^{\circ}C] = \sum Temperatures > 0^{\circ}C \quad (\text{Eq. 3})$$

The temperature curves each include their running mean with $k = 5$ a, which means that for each year the mean value of the year itself as well as the two years before and after was calculated.

As an alternative attempt to examine the connection between high temperature and rockfall occurrence, the distribution of the indicator years (cf. 6.1.2) in connection to the event years was examined and statistically tested with a Chi²-test, controlling for the independence of the variables.

Rainfall

To investigate the relationship between the event occurrence and heavy rainfall, precipitation data for each summer (June, July, August) was investigated, as rainfall happens mainly during these months. The precipitation data includes the sum of precipitation from each summer as well as the sum of days with particularly large amounts of rain, including five categories (≥ 10 mm, ≥ 30 mm, ≥ 50 mm, ≥ 70 mm and ≥ 100 mm) (Figure A. 7).

Massbalance

As another factor influenced by temperature and precipitation and as an approximation for the mass changes at the Witenwasserengletscher, summer mass balances from four glaciers in the Swiss Alps were analysed. The mass balance series are from Claridenfirn, Griesgletscher, Grosser Aletschgletscher, and Silvrettagletscher (Table 4; Figure A. 8). The Claridenfirn, Grosser Aletschgletscher and Silvrettagletscher are three of the glaciers with the longest time series of the Glacier Monitoring Switzerland measuring network (GLAMOS, 2023). The Claridenfirn is additionally situated quite close to the Witenwasserengletscher. The Griesgletscher is the closest measured glacier to the Witenwasserengletscher and has the same exposure. Claridenfirn and Grosser Aletschgletscher are southeast-exposed and might therefore show a slightly different but complementing pattern.

Table 4: Information about the four glaciers included in the mass balance series.

Name	Start of Time Series	Exposure	Remarks
Claridenfirn	1915	Southeast	Quite close to study area
Griesgletscher	1962	North	Closest to study area
Grosser Aletschgletscher	1915	Southeast	
Silvrettagletscher	1915	West	

PERMOS Database

To further investigate the relationship between climate factors and rockfall occurrence, the PERMOS database was considered, as the same influences could play a role there as for the identified events. Their timing, frequency, and volumes were compared, using the confidential, unpublished PERMOS database (PERMOS, 2023) which includes more events than the published one mentioned in the introduction.

The PERMOS database has additional variables that describe the surroundings of the events. The proportions of the variables “glacier” and “permafrost” were determined to investigate their relationship to the occurrence of rockfall events. The variable “glacier” indicates whether there is a glacier in the immediate surroundings. “Permafrost” states whether the break-off area lies within permafrost according to the SLF permafrost and ground ice map (Kenner, 2018; Phillips, 2024b).

7 Results

7.1 Identified Deposit

Rockfall deposits can be found all over the glacier. As an example of their distribution, Figure 9 displays the deposits identified in the drone image from 2022 (in green). While there are some additional deposits on the sides of the glacier (e.g. marked in orange), these could not be distinguished from each other. Furthermore, they could not be measured in the field due to safety reasons. This was also the case for deposits J and K, as well as the deposits at the top of the glacier (R, S, T, U, V). Additionally, these deposits were not connected to an isochrone and could therefore not be allocated to a year in the GIS analysis. Some of the unassigned deposits in one image could be assigned to an isochrone in another image (see “cross-dating”, Figure 8). The ones that were not connected to an isochrone in any image could not be included in the time series. Most deposits could not be identified in all images since they were not anymore or yet on the glacier’s surface at that time or too blurred to distinguish them. Table 5 shows the total number of deposits identified in each image and how many of them are connected to an isochrone.

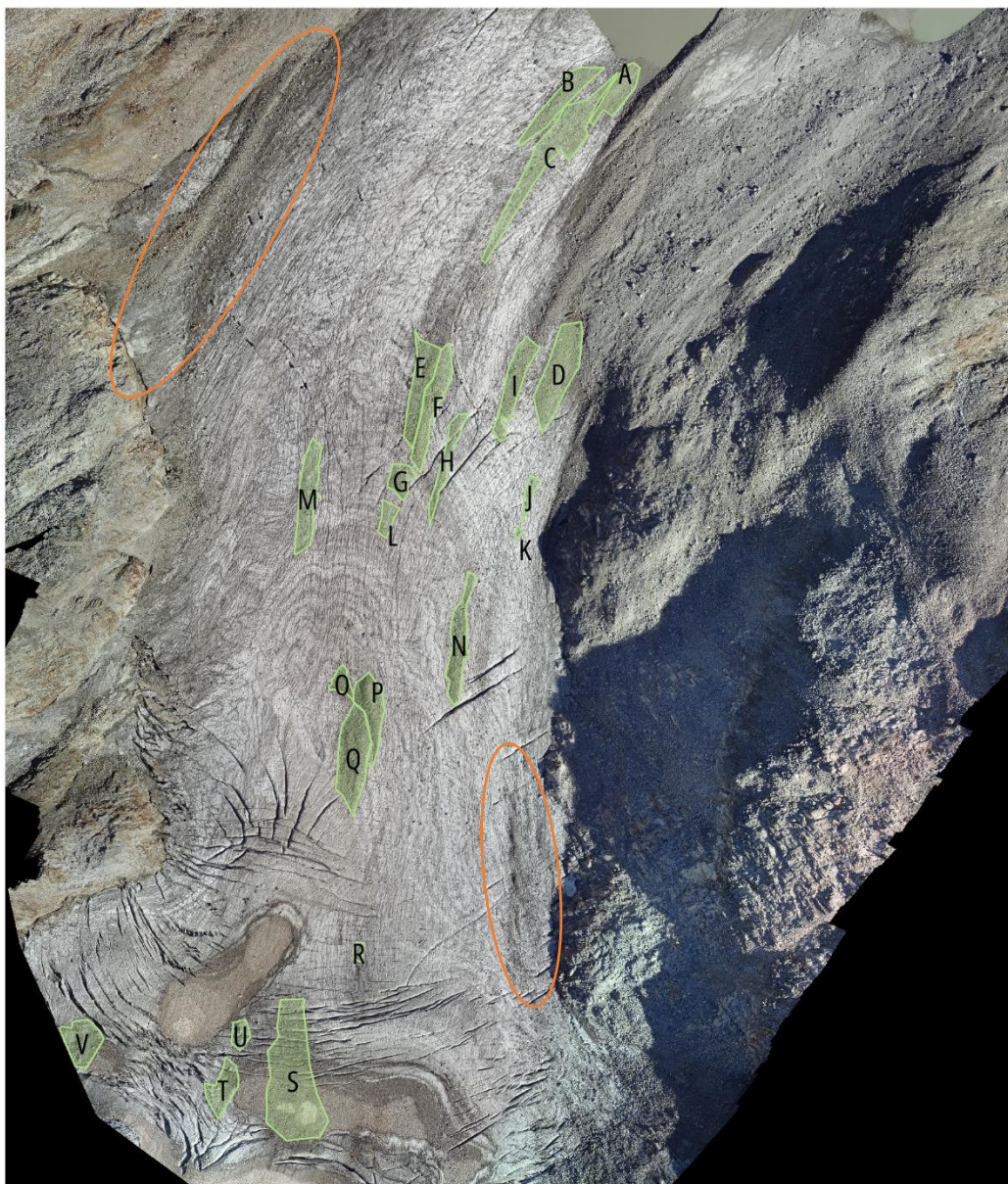


Figure 9: Section of the drone image from 2022 with the mapped deposit areas (green; A to V) and zones with additional deposits (orange) (drone image: GIUZ, 2022).

Table 5: Number of identified deposits in each image and number of deposits assigned to an isochrone.

Image	Number of identified Deposits	Number of Deposits assigned to Isochrones ¹
2022	22	9
2015	24	12
2012	14	5
2008	11	3
2003	15	12
2000	15	10

¹ Including categories "with a clear isochrone" and "with an isochrone, but unsure which one" (cf. Figure 8)

7.2 Interview with Pia Biondi

Pia Biondi, the warden of the Rotondo hut, states that there are no recorded events. She however feels that the number, intensity, and duration of “rumbling” incidents are increasing steadily. She also has the impression that the glacier becomes more and more gravelly. She further noticed that the surroundings are changing by becoming progressively more snow free and greener. Pia Biondi notes significant changes, especially from 2020 onwards, which are characterized by the occurrence of floating ice and an increased frequency and intensity of rumbling events. Further notes from the interview are provided in Table A. 3.

7.3 Identified Events and Time Series

A final time series was created based on the identification of the deposits, the isochrone counting, and the “cross-dating”. One deposit thereby corresponds to one event. The timeline has a range of 102 determined years and includes the number of events per year (Figure 10). A total of 102 isochrones, 27 events, and 24 years with events were identified. The number of events per year ranges from zero to two, with most of the years having zero events, 21 showing one event, and just three years with two events. No long-term trend, i.e. increase or decrease in rockfall activity over the entire period, could be identified. The events are clustered over time in groups of 3 – 10 years, interrupted by quiet periods of similar length (Figure 10).

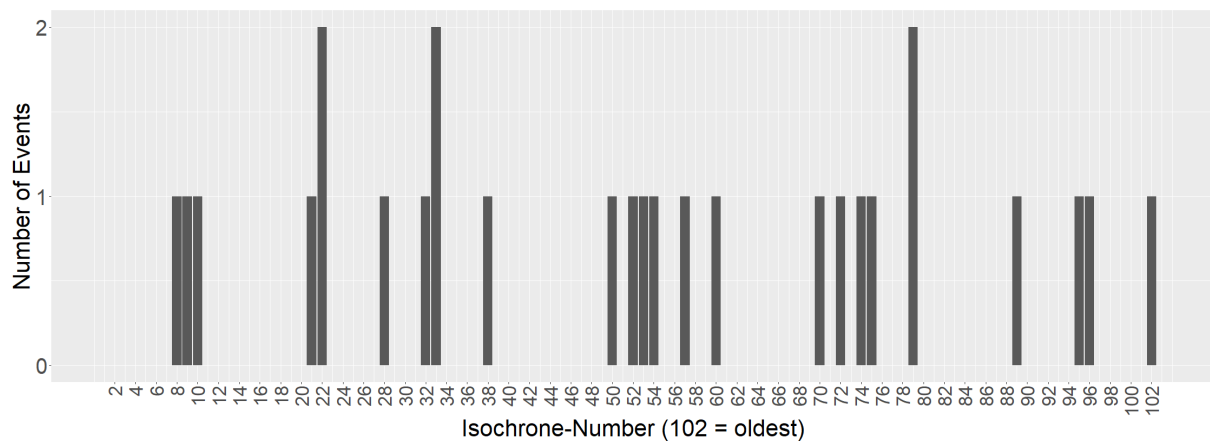


Figure 10: Timeline with the number of events per year, where 1 = youngest and 102 = oldest identified isochrone. From left to right the isochrones and events become older.

7.3.1 Allocation of Absolute Years

The scenarios identified are displayed in Figure 11 with the mean summer temperatures as a comparing factor. The events are the oldest in scenario 1994, followed by scenario “images”, scenario 2003, and finally scenario 2022 with the youngest events. The timelines lie within the range of 1906 to 2021, with a length of 102 years each. This gives us a total deviation of 13 years between the oldest and youngest scenario. From the two scenarios derived from the identification of indicator isochrones (scenario 1994

and 2003), scenario 2003 had more indicator isochrones matching with extreme years in the temperature and is therefore the more convincing scenario between the two. When comparing scenario 2022 and “images” with each other, scenario “images” is more reliable, since it considers all images. When comparing the methods of scenarios 2003 and 1994 (allocation of indicator isochrones to temperature peaks) to the ones from scenarios 2022 and «images» (counting isochrones), the latter one seems to be more reliable. Therefore, for subsequent analysis, the scenario “images” will be used. According to this the 27 events at the Witenwasserengletscher occurred between 1913 and 2014.

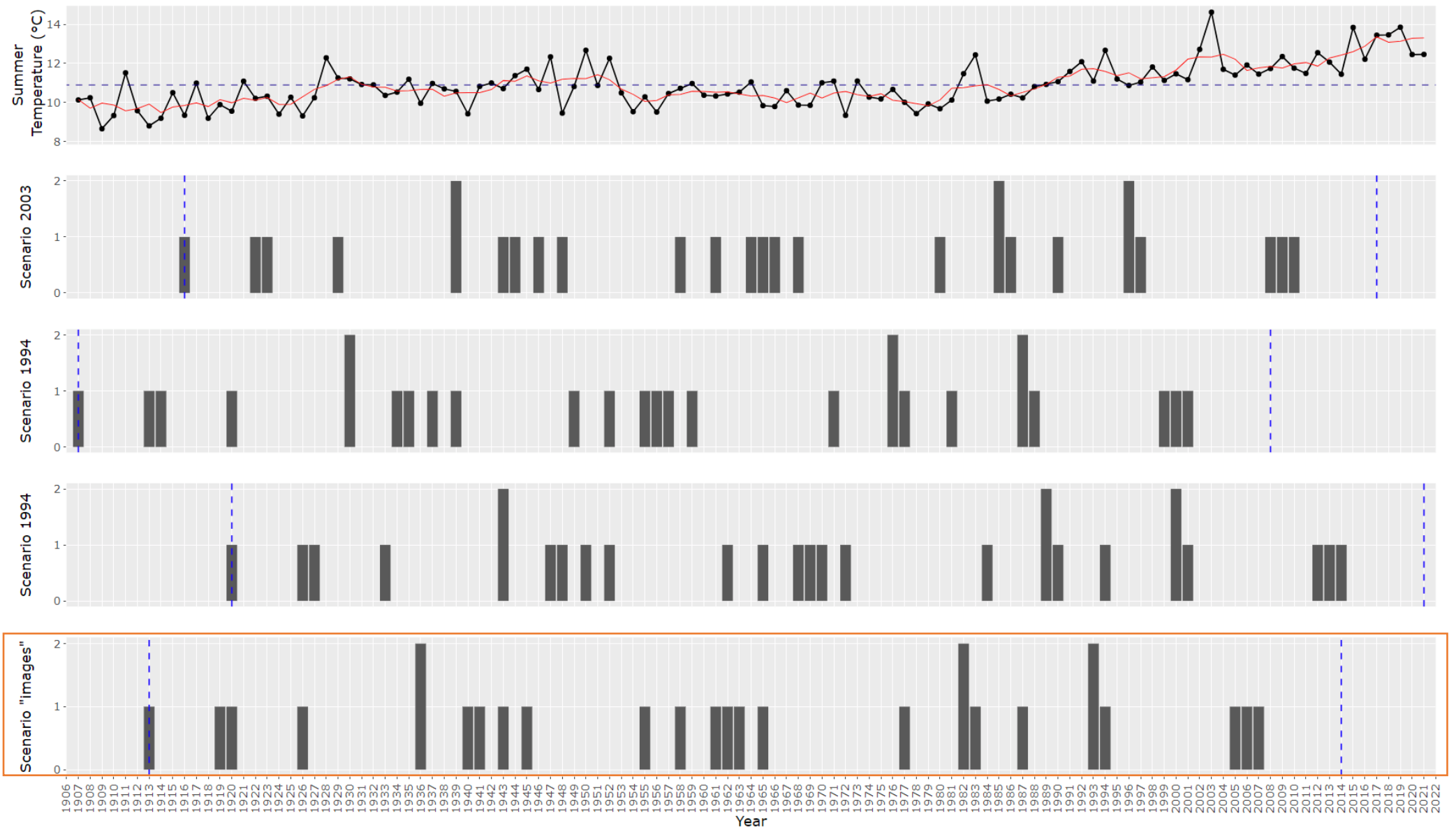


Figure 11: Number of events each year in different scenarios of absolute years, the scenario chosen for subsequent analysis is framed in orange. In the temperature plot the running mean (with $k = 5$ a) is displayed as a red line, and the mean over the whole period (1907 – 2021) as a dark blue dashed line ($=10.89^{\circ}\text{C}$). The blue dashed vertical lines in the scenarios mark the beginning and end of the isochrone recordings (first and last measured isochrone). (temperature data: MeteoSchweiz, 2023).

The search for fresh depositions on aerial images and historical photographs was unsuccessful, as none of the available images and photographs showed any deposits in the accumulation area of the glacier. Furthermore, most sources did not have any photographs or were unresponsive (see Table A. 4).

7.3.2 Properties of Rockfall Events

Figure 12 shows the determined and calculated properties of the rockfall events at Witenwasserengletscher between 1913 and 2014. 27 deposits with areas between 84 and 5312 m² were identified. Most of them are not melted out in the image they were measured in. Their thickness has values between 0.01 and 0.17 m plus one outlier of 0.5 m. The percentage coverage ranges from 10 to 100 %. The smallest percentage coverages between 10 and 20 % and one with 30 % (coloured in red) were only estimated from aerial images and not derived from field measurements. The percentage coverages and measured thicknesses combined give us values between 0.01 and 0.5 m for the mean thicknesses over the whole areas. These mean thicknesses times the measured areas lead to rounded volumes between 1 and 561 m³. The volumes are not normally distributed and small values clearly dominate (Figure 13 b)). Most of the deposits (n = 18) have volumes between 0.05 and 112 m³, five are in the range between 113 and 224 m³, and the largest four range from 225 to 561 m³. Further, the volumes do not have a long-term trend, but rather bigger events alternating with smaller events (cf. also Figure 22).

Most of the deposits have at least one image where they are visible with a definite isochrone, two are only connected to unsure isochrones and not connected to any isochrones in the other images (see also Figure 8). According to the estimated and measured rock sizes, two deposits belong to the class “very small”, five events can be classified as rockfalls, and twenty as blockfalls (Figure 13 a)). Out of the 27 deposits, nine were identified as possible rockslide events due to their total volume (≥ 100 m³). These are all classes of the equal intervals (Figure 13 b)) except those with the smallest volumes (there are no volumes between 100 and 112 m³) (marked in orange).



Figure 12: Properties of the identified events, coloured according to confidence or state of melting out, including legends. The values of the area and volume are rounded to whole numbers, and the years correspond to scenario “images”. The mean thickness corresponds to the mean thickness over the whole deposit. For better visibility, an “R” was added to the “rockfall” class in the block sizes, the smaller circles are “very small” events, and the bigger ones are “blockfalls”. The input data can be found in appendix (Table A. 5).

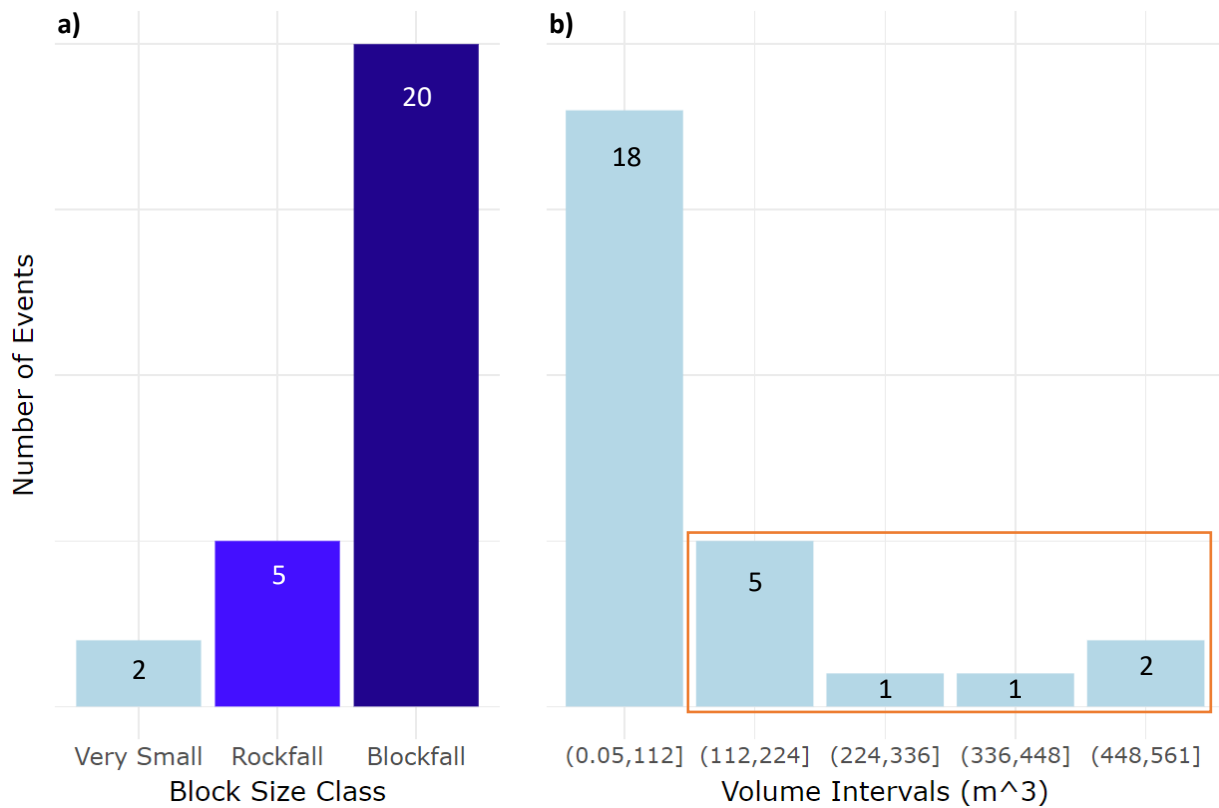


Figure 13: Histograms of the a) block size-based classes (very small < 1 m³, rockfall = blocks < 0.5 m³, blockfall = with blocks > 0.5 m³) and b) event volumes (m³) with equal interval classes. The orange square includes the events which are possibly rockslides.

Comparison Area and Thickness

For the statistical analysis of the relationship between thickness and area, a linear regression was performed between the two variables (Figure 14). The R^2 of the linear regression (= 0.022) is below 0.5 and thus indicates that the area does not depend on the thickness linearly. To get a clearer image, the investigation was done again after removing the outlier with a mean thickness of 0.5 m (Figure 15). This gave an R^2 of 0.208 (< 0.5) and therefore still indicates no linear dependency. To further analyse the relationship between thickness and area of the deposits, residual diagrams were generated (Figure A. 9; Figure A. 10), which show the deviation of each point to the linear regression. It can be clearly seen that the deviation of the three points with a large area (> 3500 m²) is very small and that there is a very large variance of the thicknesses in the deposits with areas below 3500 m². There are too few (n = 3) points with areas above 3500m² which have a small deviation and therefore influence the regression too strongly.

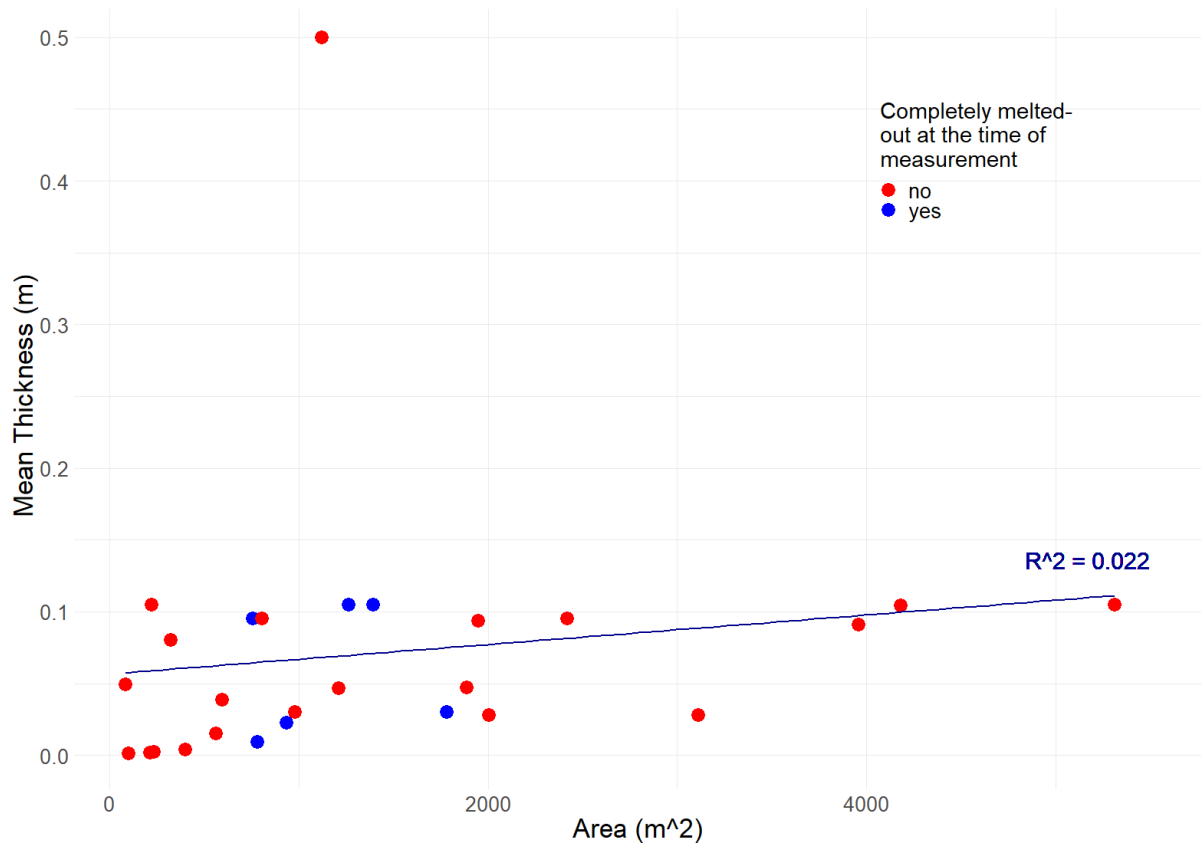


Figure 14: Comparison of the area of the deposits to the mean thickness, including a linear regression.

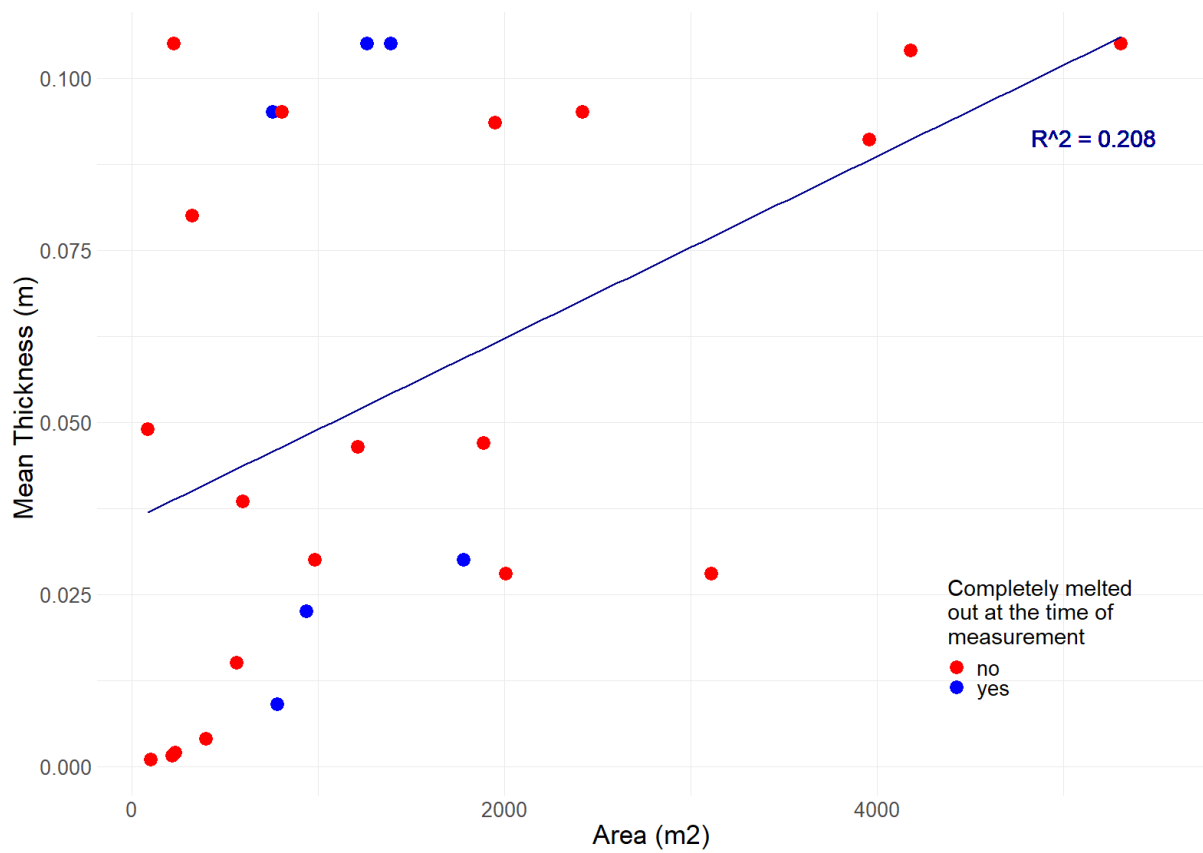


Figure 15: Comparison of the area of the deposits to the mean thickness without the outlier at a thickness of 0.5 m, including a linear regression.

7.3.3 Flow Lines and Geology

The geologies of the detected rockfall deposits identified in the field (16 out of a total of 27 events) and the determined flow lines combined with the geological map from Hafner et al. (1975) are displayed in Figure 16. The geology of the measured deposits is mostly *Zentraler Streifengneis* (blue), and some (n = 4) also contain *Rotondogranit* (orange). A24 is the only deposit consisting of only *Rotondogranit*. Deposit A13 shows big boulders of *Rotondogranit*, A6 and A15 both have some *Rotondogranit*, for all of them *Zentraler Streifengneis* clearly dominates. The other deposits (n = 11) only contain *Zentraler Streifengneis*. On the lower part of the glacier (on A4) some signs of weathering were noted.

While there are some inconsistencies, the geology of the deposits and the modelled streamlines combined with the geology according to Hafner et al. (1975) seem to match quite well (Figure 16). Most of the deposits lie within the flowlines corresponding to their geology. In the middle part, where the geologies overlap in the rock wall, most deposits only consist of *Zentraler Streifengneis*.

Legend

- Zentraler Streifengneis
- Zentraler Streifengneis (& Rotondogranit)
- Rotondogranit

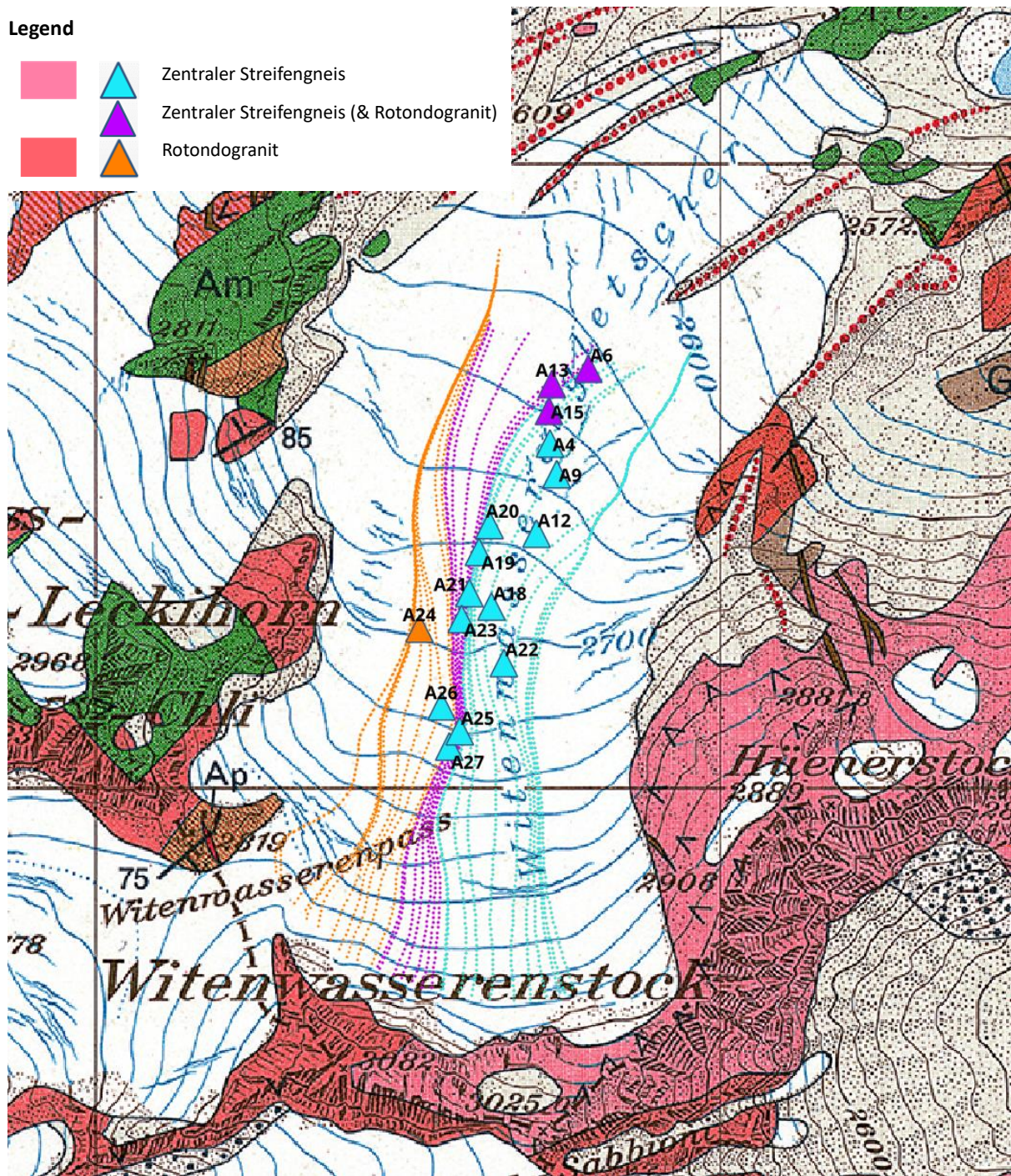


Figure 16: Flow lines on the Witenwasserengletscher (dotted lines) created with the MATLAB streamline function based on the DEM from 2019 and the identified geologies (triangles) overlaying the geological map from Hafner et al. (1975).

7.4 PERMOS Database

When looking at the timeline of the events in the PERMOS database and the events detected in this study (Figure 17), they seem to have a similar pattern. The periods with events and the periods in between (with no events) match rather well between the two datasets. Between 1920 and 1936, the years the events occurred in match perfectly. From 1966 to 1976 both datasets show a gap of events, with PERMOS having an even longer gap from 1962 to 1983. The ascending trend in the number of events after 1995 in the PERMOS data, and especially from 2003 onward, could not be seen in the identified timeline.

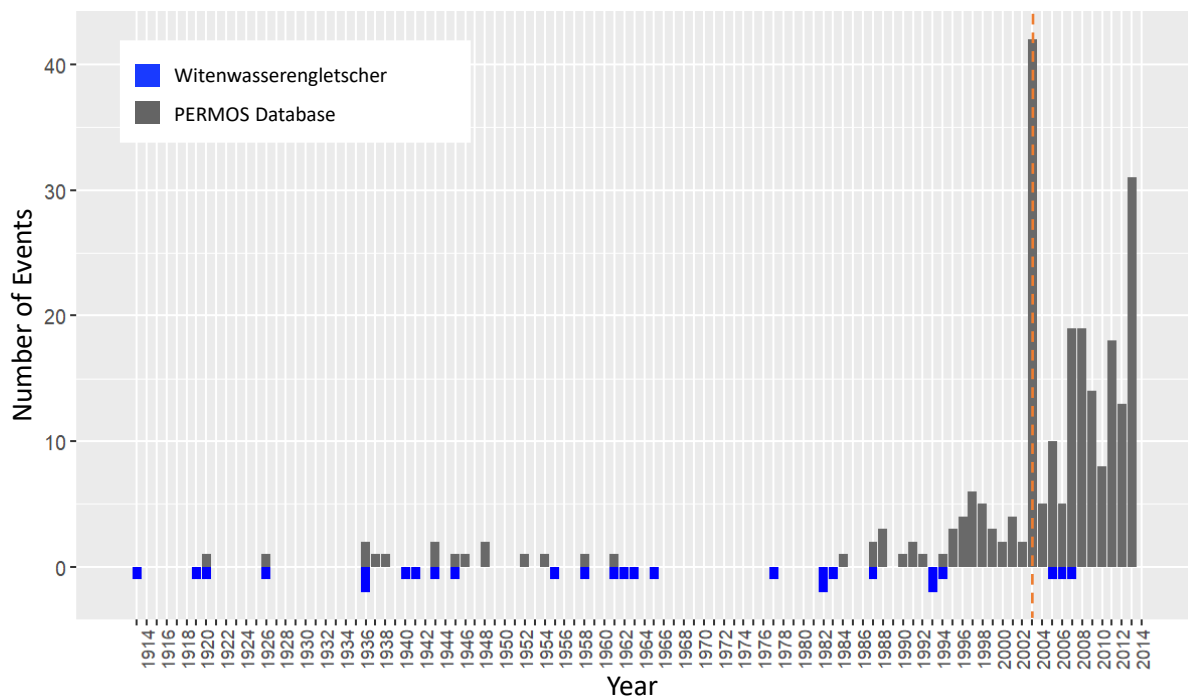


Figure 17: Timeline of the events in the PERMOS database and the events identified at the Witenwasserengletscher (flipped on the x-axis). The beginning of the active database in 2003 is displayed as an orange dashed line (data: PERMOS, 2023).

As described in the introduction (1.1) the PERMOS database is subject to a reporting bias. To reduce this bias, events in the order of magnitude corresponding to the events that were recorded early on (before 1984), were compared to the detected time series separately (Figure 18). These events have volumes greater than $100'000 \text{ m}^3$ (cf. Figure 19). The upgoing trend in the PERMOS database is less obvious here. The periods with and without events match even better, especially in the last 20 years. The identified event cluster from 2005 to 2007 matches perfectly with a peak of events greater than $100'000 \text{ m}^3$ in the PERMOS dataset.

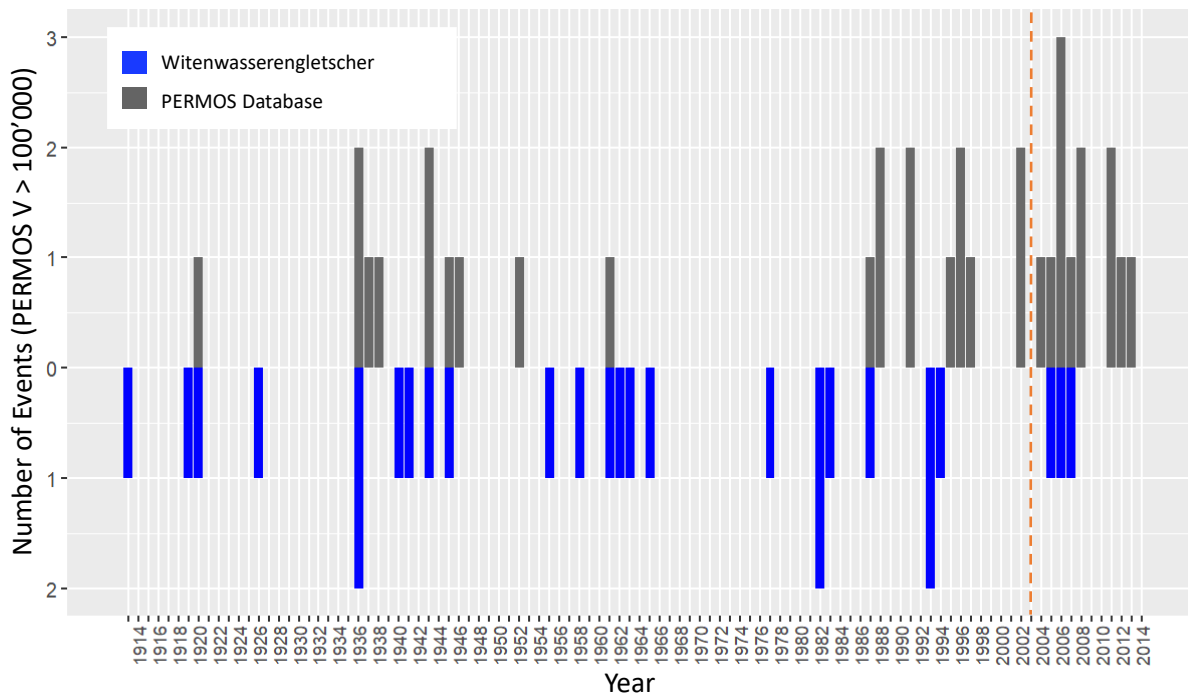


Figure 18: Timeline of the events in the PERMOS database (events with $V > 100'000 \text{ m}^3$) and at the Witenwasserengletscher (flipped on the x-axis). The beginning of the active database in 2003 is displayed as an orange dashed line (data: PERMOS, 2023).

The volumes of the investigated deposits and the events from the PERMOS database are presented in Figure 19. The volumes of the measured deposits are smaller than the ones in the PERMOS database. Some of the newer events, since 1999, in the PERMOS database match with the order of magnitude the bigger measured events have. However, most of the measured events are even smaller.

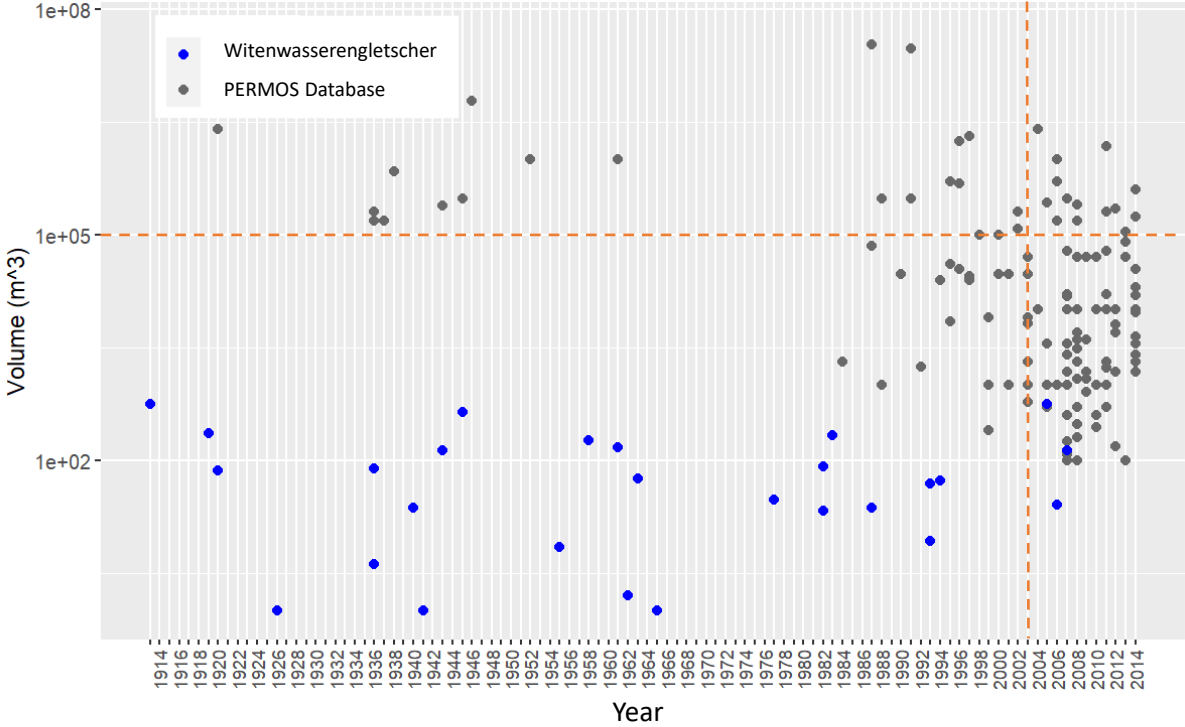


Figure 19: Volumes of the measured deposits and the events in the PERMOS database on a logarithmic scale. The start of the active PERMOS database (vertical) and the volume threshold (horizontal) are marked as an orange dashed line (data: PERMOS, 2023).

Figure 20 shows (a) the proportion of the events in the PERMOS database which occurred from a permafrost region according to Kenner (2018) and (b) the proportion of glaciers in the immediate surrounding of the rockfall events included in the PERMOS database (PERMOS, 2023). For more than half of the events, the break-off zone was a suspected permafrost rock wall. Almost one third of the events did not originate from a permafrost rock wall. A large proportion is also unknown. Almost 2/3 of the rockfall areas do not have any glaciers nearby. About one quarter does or possibly does have a glacier in the close surrounding possibly influencing the rockfall occurrence according to PERMOS (2023). There is a large proportion of events with no data on the presence of glaciers nearby.

a) “Permafrost” in the PERMOS Database b) “Glacier” in the PERMOS Database

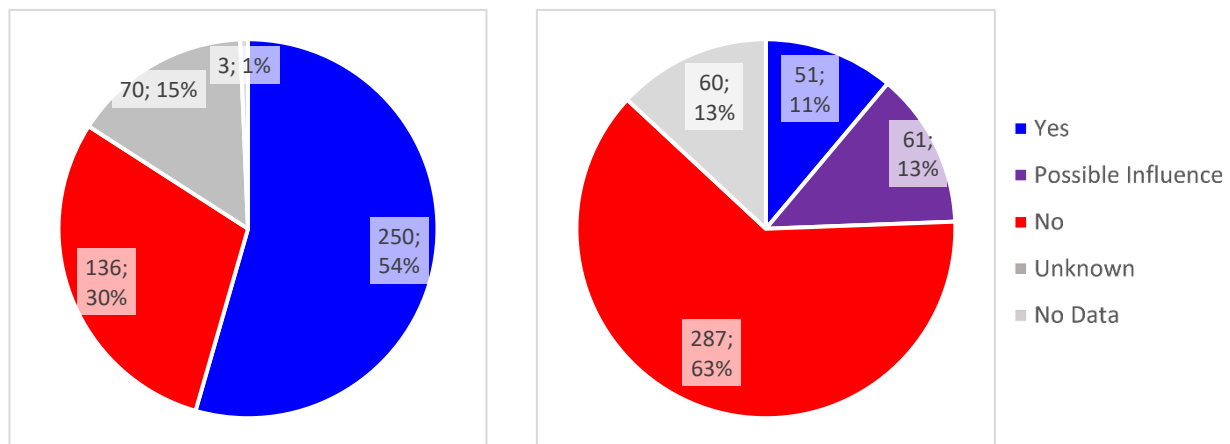


Figure 20: Proportions of the variables a) “glacier” (= glacier in immediate surroundings of rockfall events) and b) “permafrost” (= permafrost occurrence at the events according to Kenner (2018)) in the PERMOS database (n = 459). The category “yes” in subplot a) includes two events with “yes, partially” (data: PERMOS, 2023).

7.5 Climate Variables

The PDD, annual mean temperature, mean summer temperature, summer ablation, summer precipitation, and detected rockfall time series from Witenwasserengletscher are displayed in Figure 21. All temperature variables (mean annual temperature, mean summer temperature, PDD) and the summer mass balance show a similar pattern. They all have an increasing long-term trend, especially from 1990. Their peaks are mostly in the same years and are most pronounced in the summer temperature. This shows that the mean summer temperature has a strong influence on the other factors and can be taken as an approximation for the mean annual temperature, the PDD, and the summer mass balance. For better visibility, subsequent analysis on these variables will therefore be done only with the mean summer temperature. The precipitation data follows another pattern with no long-term trend, and will therefore be compared to the detected time series separately.

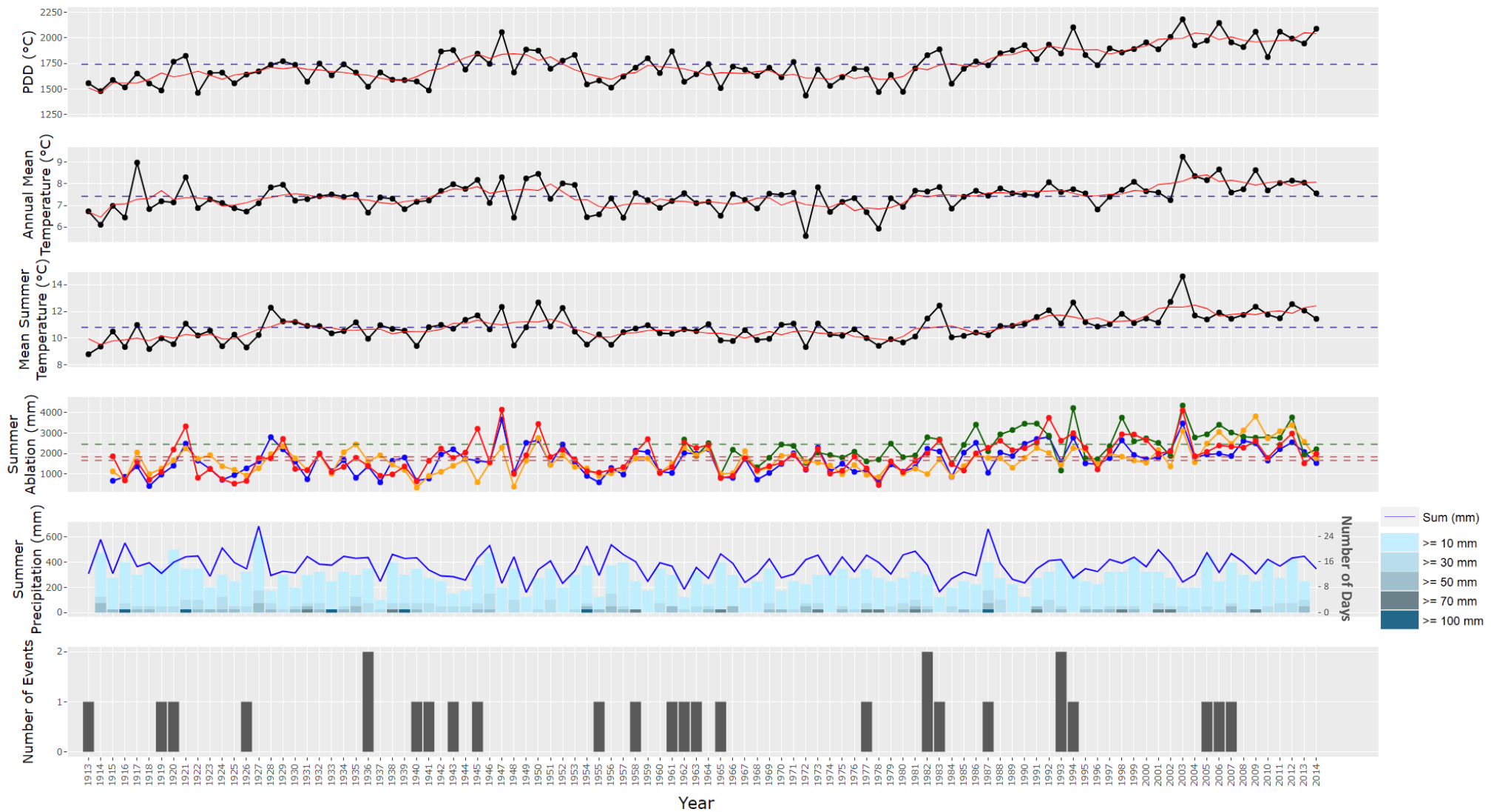


Figure 21: PDD, annual mean temperature, mean summer temperature (all three including their mean over the whole period as a blue dashed line and running mean with $k = 5$ in red), summer ablation of the Claridenfirn (blue), Griesgletscher (green), Grosser Aletschgletscher (orange) and Silvrettagletscher (red), summer precipitation including the total summer precipitation (sum) and the number of days with high amounts of rainfall, and detected rockfall time series from Witenwasserengletscher. The individual climate variables can be viewed in the appendix (Figure A. 4 – Figure A. 8; precipitation and temperature data: MeteoSchweiz, 2023; mass balance data: GLAMOS, 2023).

7.5.1 Mean Summer Temperature

The mean summer temperatures in comparison to the event occurrence and their volumes are displayed in Figure 22. On first impressions, peaks are visible in all three plots. In 1983, the volume and temperature peak match perfectly. In the other years the general pattern is similar, but the exact years do not match.

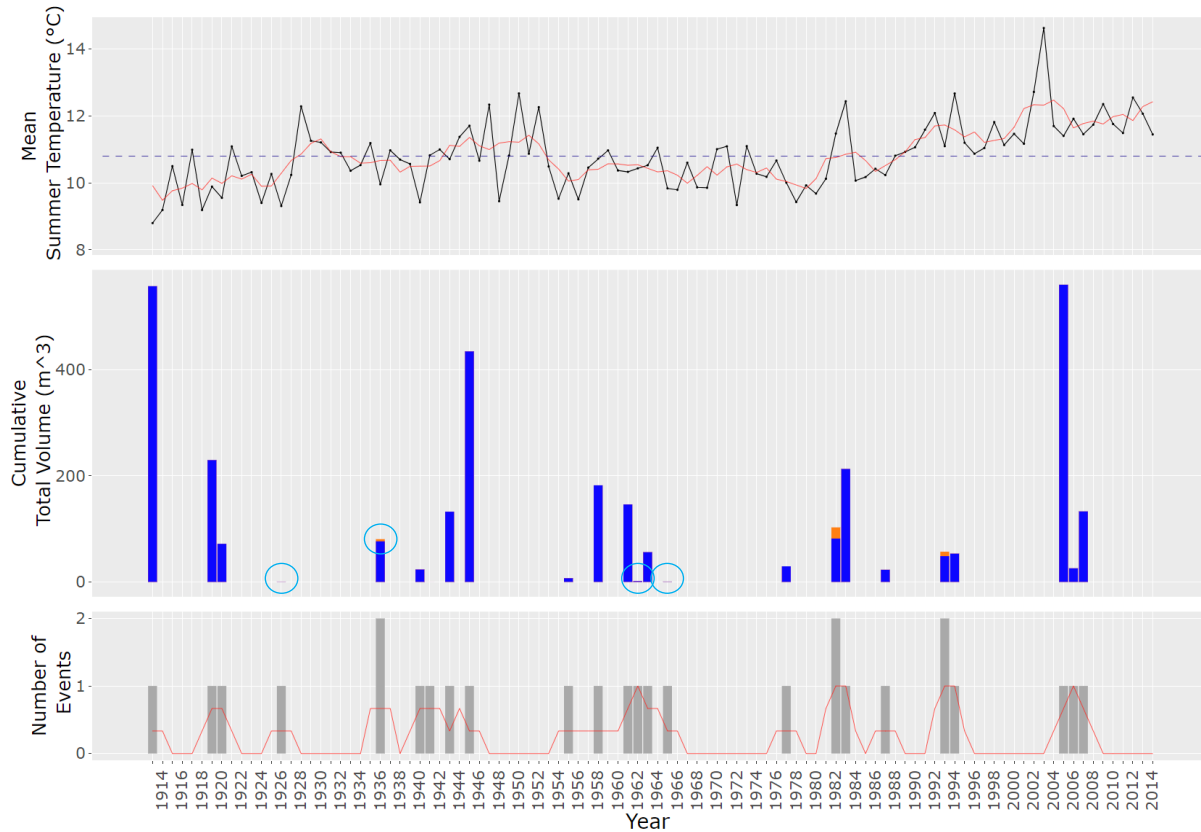


Figure 22: Summer temperature, event time series and volumes of the events over time, with the running means in red (temperature $k = 5$ a; events $k = 3$ a) and the mean of the temperature from 1910 to 2017 ($=10.85^{\circ}\text{C}$) in dark blue and dashed. The volumes of two events in one year are cumulated, and the volumes of the second deposits are displayed in orange. For better visibility, the smallest volumes are circled in light blue (temperature data: MeteoSchweiz, 2023).

7.5.2 Indicator Isochrones

Figure 23 shows the identified indicator isochrones, as well as years with events and their overlap. The indicator isochrones are especially dirty (nr. 22, 33 and 38 (dirty & thin)) or thin (all others) and therefore represent years with particularly warm temperatures. The indicator isochrones are, like the detected events, clustered with gaps of 5 to 10 years in between and appear in pairs (two consecutive years) or isolated. Out of the 102 isochrones, 12 were identified as indicator isochrones, and six of those also have events. Two indicator isochrones lie next to an event year (one year before or after). 18 isochrones had events but were not identified as indicators.

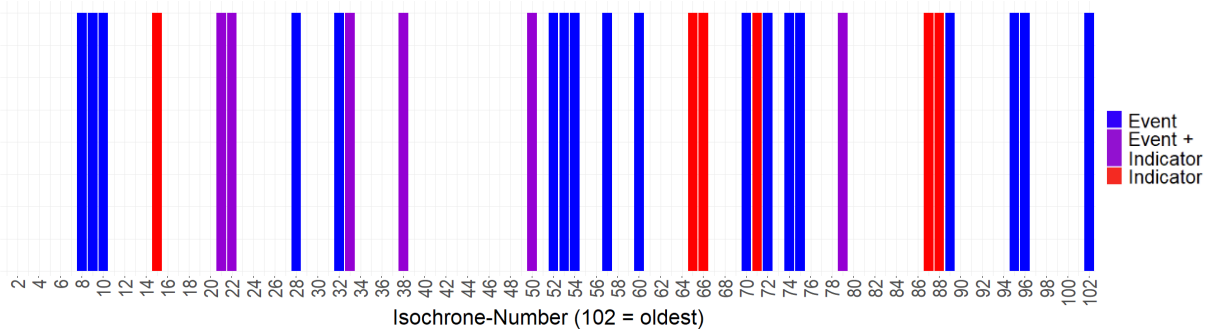


Figure 23: Timeline with the identified indicator isochrones and the years with deposits.

In the pie chart (Figure 24 a)) the fractions of the different categories in proportion to all years are presented. It can be seen again that half of the indicator isochrones also have events. In total, a bit more than a quarter of all years belongs to one of the categories. In Figure 24 b), the indicator years that lie one year before or after an event are also included in the category “Event and Indicator”. The proportion of this category is even higher here. Two-thirds of the indicator isochrones are exactly in the same year or one year before or after an event year. Only one-third of the indicator isochrones is without an event year.

Proportions of Event and Indicator Years

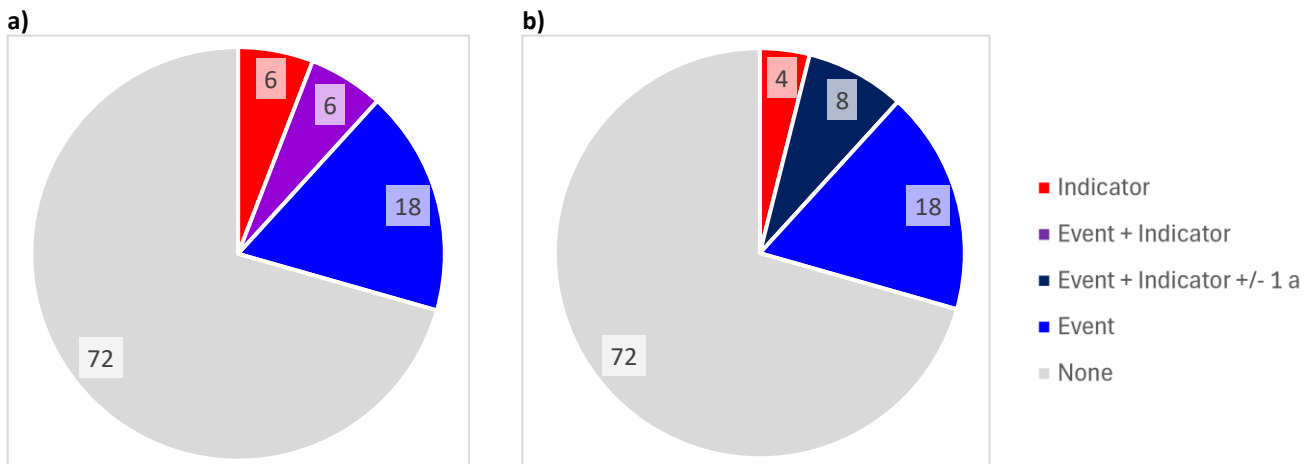


Figure 24: Proportions of the indicator years, rockfall event years, and indicator years with events, a) as identified and b) including the indicator years one year before or after an event ($n = 2$) in the category combining the two variables (total = 102 years).

The Chi² test, which was performed to determine the relationship between the occurrence of events and indicator years, tested whether these two variables are independent (= null hypothesis). The test gave a Chi² of 5.3 and 12.1 for the distributions in Figure 24 a) and Figure 24 b) respectively. The Chi² of 5.3 is greater than 5.0 (critical value for significance level of 2.5 % with a degree of freedom of 1; DATAtab, n.d.) and the null hypothesis can therefore be rejected with a significance level of 0.025 (= 2.5 %). With a Chi² of 12.1, the significance level for the distribution including indicator years before or after an event year (Figure 24 b)) is even higher with 0.1 % (critical value = 10.8; DATAtab, n.d.). The null hypothesis can therefore be clearly rejected, meaning that the event and indicator years are not independent of each other.

7.5.3 Summer Precipitation

Since Figure 21 already reveals that the sum of the summer precipitation has no similarities to the rockfall time series, the detected rockfall time series will only be compared closer to the number of days with extreme precipitation. Additionally, single events of heavy rainfall are expected to influence the rock wall stability, which are not represented in the sum of precipitation over the whole summer (June, July, August). Figure 25 was therefore created to compare the number of days per summer with extreme precipitation to the identified rockfall event timeline. While there is no obvious relation between the two variables, there seems to be some consistent patterns. One year that stands out immediately is 1987. In this year, a rockfall event was detected and a day with more than 100 mm of rain as well as several days with more than 50 mm and more than 30 mm occurred. In 1958, 1965 and 1977 rockfall events occurred in the same year as daily precipitation events above 70 mm. 2007 also shows an event and two days with more than 50 mm precipitation. These give a total of 5 years out of 24 “event years” which could indicate a connection between the occurrence of events and extreme precipitation. However, 5 out of 6 years with a day with more than 100 mm precipitation have no events and 10 out of 13 years with a day with more than 70 mm precipitation.

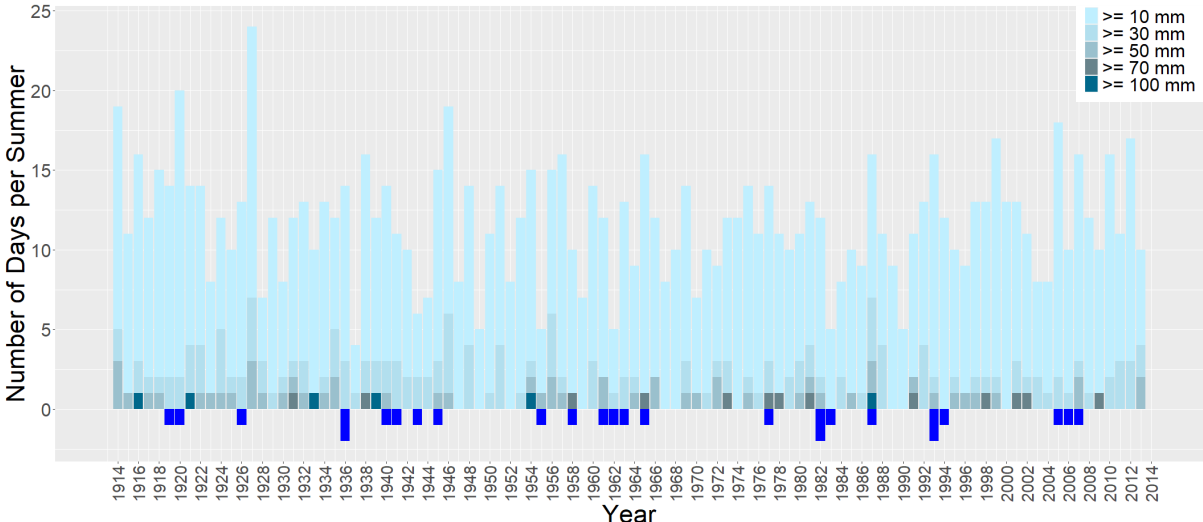


Figure 25: Number of days with extreme precipitation in the summer months (June, July, August) in Andermatt and the detected event timeline (flipped on the x-axis) (precipitation data: MeteoSchweiz, 2023).

8 Discussion

8.1 Reconstruction of Rockfall Events (Research Question 1.)

The identification of 27 events between 1913 and 2014 confirms that rockfall events in the catchment area of the Witenwasserengletscher (UR) over the past century can be reconstructed from deposits on the glacier. The quantity and quality of available aerial images, however, limits the temporal extent of the analysis to 102 years. Further, it must be noted that only deposits from the headwall can be reconstructed with the applied methods as they have to be deposited in the accumulation area for them to be connected to an isochrone (cf. Figure 2).

8.1.1 Frequency and Timing of Rockfall Events (Research Question 1.1)

The investigation of the temporal pattern of the rockfall events (Figure 10) revealed that there is no long-term trend, i.e. increase or decrease in rockfall activity, over the entire investigated period. This would have been expected according to previous literature suggesting that with rising temperatures, due to human-induced climate change, rockfall events occur more frequently (e.g. Noetzli et al., 2003; Ravanel & Deline, 2010; Street et al., 1990) due to (i) permafrost thawing (e.g. Allen & Huggel, 2013; Gruber et al., 2004; Gruber & Haeberli, 2007; Noetzli et al., 2003; Ravanel & Deline, 2010; Street et al., 1990; Streletskiy et al., 2015), and (ii) debulking due to glacial retreat (e.g. Ballantyne, 2002; Haeberli et al., 2013; McColl, 2012). Additionally, the exposure of the headwall by glacier thinning would further increase the area and hence the rate of rock wall erosion (Bolch & Christiansen, 2015; Deline et al., 2015). Therefore, more and/or larger rockfalls would have been expected as time goes on. The lack of a long-term trend in the identified rockfall time series does however not support these hypotheses. The statements from the interview with Pia Biondi, the warden of the Rotondo hut, which correspond with observations during the field work, would indicate an increase in the number of incidents. These are however mostly individual stones that detach from the side wall (especially Läckihorn; Figure 6 c)) and were therefore not included in the detected rockfall time series.

An uncertainty in the rockfall time series occurs from the identification of the isochrones due to missing or doubled rings. Missing rings can occur when there is not enough accumulation or too much ablation leading to the entire snow from one year (or more) melting and thus not building a layer. Doubled rings can develop when there is a second layer in a snow rich summer that is not compressed enough, leading to two visible isochrones in one year. Furthermore, the identification of isochrones and the allocation of the events to the isochrones can be challenging. The visibility classes and cross dating were used to evaluate and minimize this uncertainty. Deposits A9 and A10 could not be definitively assigned to an isochrone in any image, leading to a possible shift in their temporal occurrence.

While the relative timeline of the rockfall events is well constrained, it is non-trivial to assign an absolute timescale to the events. To identify absolute years, four scenarios were considered (Table 2; Figure 11). As described in the results section (7.3.1), scenario “images”, which was determined by counting the isochrones from the topmost visible isochrone in all images, was identified as the most reliable scenario, and was therefore used for subsequent analysis. Nevertheless, some uncertainty still remains for scenario “images”. During the identification of the scenario, the years did not match up between all images. This was most likely due to isochrones being covered by snow or melted away. In the drone image from 2022, the topmost isochrone was defined as 2014 in scenario “images”, which means seven years were melted away, as it would otherwise have been 2021 (one year before the image was taken; cf. Figure 2). For the absolute time series, the oldest age was taken, since it does not contradict the younger ones and matched with the most images. This means it is unlikely that the events are younger, which would contradict most of the ages identified, and therefore a minimum age was determined.

8.1.2 Sizes of Rockfall Events (Research Question 1.2)

When looking at the sizes of the events, there is a wide range of areas, percentage coverages, and thicknesses (Figure 12). The final volumes range between 1 and 561 m³, where most deposits are not fully melted out and these values therefore represent a minimum volume. Note that the order of magnitude of the deposit volume does not depend much on the state of the melt-out (Figure 12; Figure 14). Some densities and thicknesses were estimated from aerial images and not measured in the field, which makes the volumes calculated on their basis less secure.



When analysing at the mean thickness over the whole area, there is an outlier with a value of 0.5 m (see Figure 14). This deposit (A25) has the largest volume even though the melted out area is quite small. The exceptionally high density and thickness are visible in the picture of the measured square (cf. Figure A. 3) as well as in the cutout of the drone image from 2022 (Figure 26). This effect is exacerbated by reduced melting under the thick debris cover (e.g. Mattson et al., 2008).

Figure 26: Cutout of the drone image from 2022 with deposits A25, A26 and A27 (GIUZ, 2022).

The area does not depend on the thickness (Figure 14), even when analysing this relationship without the outlier with a thickness of 0.5 m (Figure 15). The volume can therefore not be derived directly from the area measurement. This means thickness measurements, especially the exact ones from the field recording, are still needed to determine the volumes of rockfall events.

The division of the events into the block size-based categories (i) very small ($n = 2$), (ii) rockfall ($n = 5$) and (iii) blockfall ($n = 20$) showed that most of the events are blockfalls (Figure 13 a)). Further, nine of the 27 events were categorized as rockslides based on their total volume according to the definition from SLF (n.d.). This number could be even higher considering most of the deposits were not melted out completely when their area was measured. When considering that there were events with large blocks (= blockfalls) and of this extent (classified as rockslides), it seems surprising that none of them were documented.

8.1.3 Geology and Breaking Point of Rockfall Events (Research Question 1.3)

The geological composition of the rockfall events at Witenwasserengletscher is clearly dominated by *Zentraler Streifengneis* (Figure 16), likely originating from the same part of the headwall. The field notes indicate signs of weathering for deposits at the lower part of the glacier (e.g. rockfall event A4), which could be because these deposits have been on the glacier for a long time and thus exposed to weathering.

To reconstruct the breaking point of the rockfall events, the geologies identified in the field as well as the streamlines were consulted (Figure 16). Since the geology was measured in the field and the two rock types (*Rotondogranit* and *Zentraler Streifengneis*) are clearly distinguishable, this source seems more reliable compared to the streamlines. The deviations of the streamlines are likely due to topographic changes over time, which could be reduced by combining DEMs from different years to determine the transport routes. However, given the expected geologies based on the transport routes of the rockfall events match well with their geologies identified in the field, the streamlines seem to be a good approximation for the breakout zones already. This means that the breakout zones of the deposits not measurable in the field could be reconstructed from streamlines representing the transport routes of the deposits. To get a clear image of the origin of the rockfall events, it is best to combine the streamlines with field measurements, as shown in Figure 16.

8.2 Comparison to PERMOS Database (Research Question 2.)

According to the detected rockfall time series, the rockfall events on the Witenwasserengletscher agree with periods of increased events in the PERMOS database (Figure 17), at least until 1994. Between 1960 and 1985, more events were identified in this study than were registered in the PERMOS database. This could be due to a lack in the occurrence of big events or events at well-investigated sites.

Particularly before the 2000s, the PERMOS database predominantly recorded larger events, which were more likely to be recorded, even before the start of the active database. This means that the event frequency before the 2000s is likely underestimated in the PERMOS database and more complete at the Witenwasserengletscher.

The increase in rockfall events in the PERMOS database after 1994, especially from 2003 when the database was implemented, is likely overestimated through an elevated reporting rate (Phillips, 2024a). This becomes evident when looking at the sizes of the reported events, with a clear increase in smaller events from about 2005 on (Figure 19). This could explain the lack in a long-term increasing trend in the identified time series, as the PERMOS database is subject to a reporting bias. However, it is also possible that the headwall at the Witenwasserengletscher had to build up enough weakened material between the events. As this takes time, it is not possible to have as many events in one place proportionally to a big area with lots of rock walls (i.e. the Alps). The alternation of bigger and smaller rockfall events in the detected time series (cf. Figure 22) could also be an indication of this.

The discussed reporting bias in the PERMOS database overestimates the rockfall event occurrence after the 2000s while also making the database incomplete before then. The investigation of the occurrence of mainly smaller events from deposits on a glacier therefore results in a time series which corresponds better with reality.

To try to avoid the reporting bias, only PERMOS events with volumes $> 100'000 \text{ m}^3$ were looked at (Figure 18). These big events are noticed even when fewer people go to the mountains. Therefore, big events are better comparable to the time series detected in this study. When matching this subset of the PERMOS database to the detected rockfall time series, they match even better compared to the entire PERMOS database. This shows once again that the frequency and number of events in the PERMOS database after 2003 is overestimated. When considering the events before the 2000s, the two time series might match even better with a shift of a few years in the detected rockfall timeline.

The observations made suggest that even though the patterns of the two time series appears a bit different in the previous 21 years, they are overall quite similar. This leads us to the conclusion that with small events from one location, you get a similar temporal distribution as with large events from a larger area. Furthermore, the agreement between the two rockfall time series could be an indicator for a common cause (high temperature or heavy rainfall).

The great proportion of PERMOS rockfall events recorded from breakout zones in expected permafrost indicates a potential link between the presence of permafrost and rock fall events. This is also consistent with detected events in this study, since they originated from a rock face that is likely in permafrost according to the SLF permafrost distribution model (Kenner, 2018; Figure A. 1) which was

also used for the classification in the PERMOS database. The presence of permafrost, however, does not indicate a direct relationship between the stability of permafrost walls and climate (high temperatures or heavy rainfall). It could however point out a common cause, namely permafrost thawing, for the events in both databases.

The proportion of one fourth of the events in the PERMOS database with a glacier in the immediate surrounding is consistent with the percentage presented in literature (Deline et al., 2015; Evans & Delaney, 2015). This variable is interesting because of the glacier retreat and its influence on the stability of rock walls (Phillips, 2024b). However, its great proportion and the agreement with literature does not confirm that the rockfall events were influenced by a glacier.

8.3 Comparison to Climate Variables (Research Question 3.)

8.3.1 Temperature

The temperature variables (mean annual temperature, mean summer temperature, and PDD) and the summer mass balance of other Swiss alpine glaciers are represented by the mean summer temperature (cf. 7.5). Therefore, its relationship with the occurrence of rockfall events discussed below applies to all these variables, unless specifically mentioned otherwise.

As discussed in the introduction and theoretical background, there are several studies concluding a relationship between high temperatures and increased rockfall frequency (e.g. Allen & Huggel, 2013; Gruber et al., 2004; Gruber & Haeberli, 2007; Noetzli et al., 2003; Ravanel et al., 2017; Ravanel & Deline, 2010; Street et al., 1990). As extremely warm temperatures have increased in the past century, especially since 1950 (IPCC, 2021), it would have been expected that the temperature variables as well as the detected rockfall time series show an increasing long-term trend. This is the case for the temperature data. However, it only gets more profound from 1990 (Figure 21). The lack of a long-term trend in the identified rockfall time series, shows that the connection between high temperatures and rockfall occurrence in this study is not that eminent.

When further investigated, the clustering of the events could be an indicator of a connection between the event occurrence and fluctuations in summer temperature. An approach was made to match the clusters of the detected rockfall event timeline with peaks in summer temperatures (cf. “wiggles matching”). This shows that there is the same number of peaks in the rockfall time series and the summer temperature during the investigated period. Further, the periods of increased rockfall activity could be allocated to peaks in summer temperature (Figure 27). The PDD and mean annual temperature have a peak in 1920 that does not exist in the summer temperature. In this year especially warm days occurred outside of summer (June, July, August). The detected events in 1919 or 1920 could have also been triggered by this especially warm year. The allocation of the periods with increased

rockfall activity to peak clusters in the summer temperature (Figure 27) shows that there are clusters that align well, and others that are shifted in time. The detected rockfall events in 1982 and 1983 match perfectly. In general, the newer events from 1977 onwards have a shift of only a few years. The older the deposits are, the greater the shift becomes. This makes sense, since the offset might partly be a result of missing isochrones, errors in the identification of isochrones, or inaccuracies in assigning absolute years. These errors cumulate over time. A temporal lag between high temperatures and the reaction of the rock wall stability (Deline et al., 2015) might be another reason for the delay. It is therefore more likely that the events occur after the peaks in summer temperature (green bars) than before (violet bars). The allocation in Figure 27 shows that the occurrence of rockfall events is presumably influenced by high temperature and will therefore likely increase with rising temperature x due to human-induced climate change (IPCC, 2007).

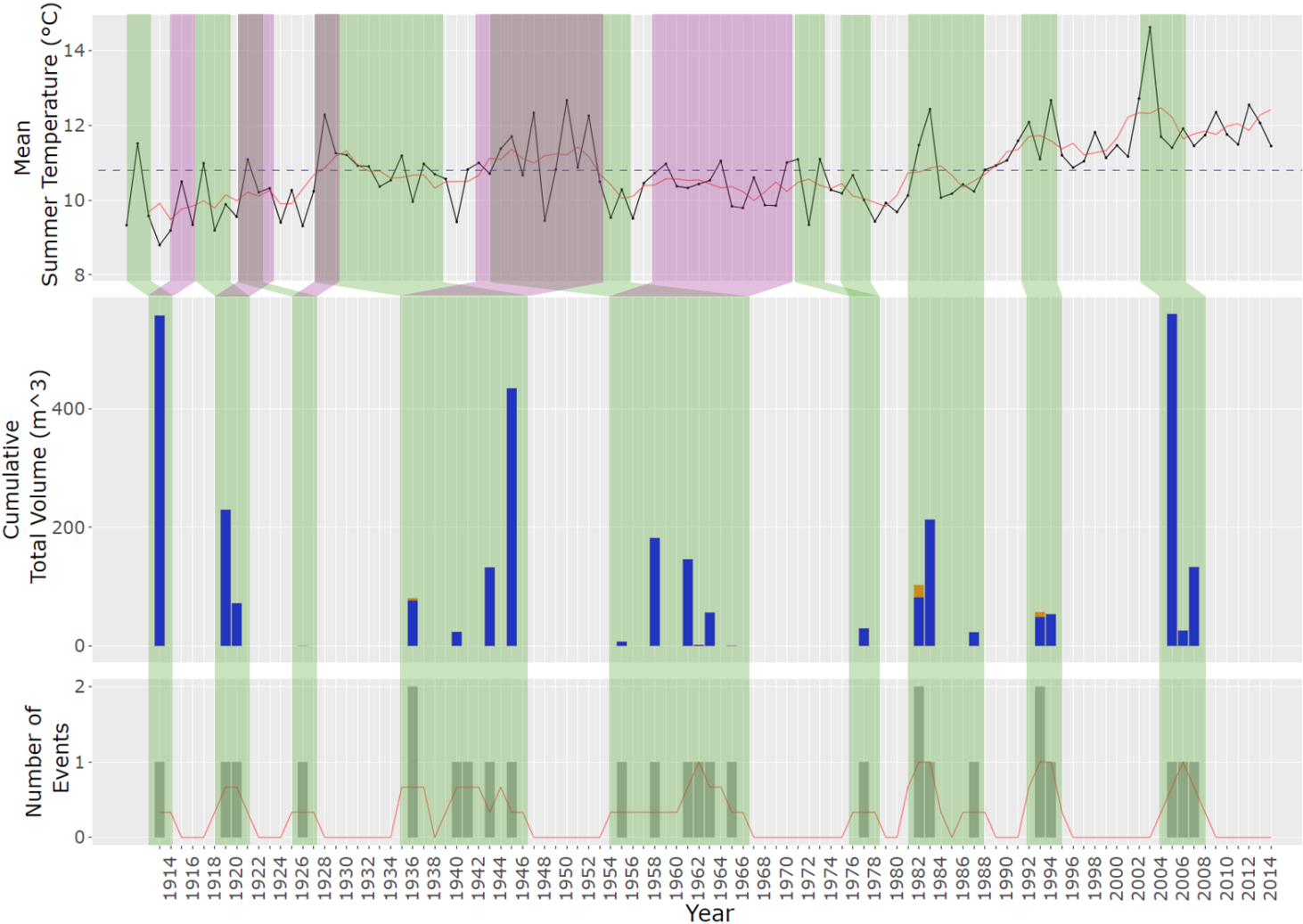


Figure 27: Allocation of the periods with increased rockfall activity to peaks in summer temperature (“wiggle matching”; in green and violet) including the mean of the summer temperature per year (in black), event time series, and volumes of the events over time. With the running means in red (temperature $k = 5$ a; events $k = 3$ a) and the mean summer temperature over the whole period ($=10.81^{\circ}\text{C}$) as a dark blue dashed line. The volumes of two events in one year are cumulated, the volumes of the second deposits are displayed in orange (temperature data: MeteoSchiweiz, 2023).

An additional explanation for the quiet periods between phases with increased rockfall activity could be the exhaustion of the rock wall from detachable or thawed material. The concept behind this is that the rock wall does no longer have enough fractured and loose material immediately after events and time is required to weaken and weather part of the rock wall enough to fail again. However, this theory remains speculative, and no previous studies could be found confirming this.

Indicator Isochrones

An alternative and independent approach to finding a possible relationship between the event timeline and extreme temperatures was made by identifying indicator isochrones and linking them up with event years (Figure 23). In this approach, the extremely warm years and event years can be compared without knowing an absolute year. Therefore, it does not matter whether the isochrones were allocated to the correct absolute year and whether the number of isochrones between the events was right. As presented in the results, these two variables match together quite well. Half of the indicator isochrones identified match with an event year exactly (Figure 24 a)) and in two thirds of the extreme years an event occurred in the same year or the year before or after (Figure 24 b)). Events occurring in the year after an indicator year could again be due to a temporal lag between high temperatures and the occurrence of rockfalls (Deline et al., 2015). The χ^2 test also confirms that the indicator isochrones and event years are not independent and that these two factors are related. This indicates a substantial connection between extremely high temperatures and the occurrence of rockfall events.

8.3.2 Rainfall

The summer precipitation shows a different pattern than the temperature data and, like the detected rockfall time series, does not reveal a long-term trend.

The comparison of the event timeline to the number of days with extreme precipitation during summer (Figure 25) shows an agreement in 5 out of 24 event years in a total of 102 years. This does not indicate any direct dependency. Inversely, most of the years with a day with heavy precipitation do not have events. This leads us to believe that there is no relationship between extreme precipitation and rockfall event occurrence at the Witenwasserengletscher on an annual basis. It is therefore suspected that an investigation with a temporal resolution of a year for the rockfall occurrence might not be effective when investigating the connection to heavy rainfall. This makes sense when considering that rainfall is a triggering factor, and therefore short-term changes are crucial. This could also be a reason that the comparison to the total summer precipitation (Figure 21; blue curve) did not reveal any correlation to the rockfall occurrence.

Further, the available precipitation data was collected at the meteorological station in Andermatt and not directly at the study site. This can lead to uncertainties due to local differences in precipitation, which can be particularly large in alpine regions (Wastl & Zängl, 2008; Zängl et al., 2008). These local differences could not be considered in this study.

8.4 Outlook

Since the investigation relies mainly on aerial images, it can be reproduced even after the glaciers and deposits have disappeared. Moreover, additional approaches could be used to confirm the applied methods and further investigate the relationship between rockfall occurrence and climate variables.

To minimize the error of isochrone identification even more, several people could do the same analysis and compare their results. Alternatively, an automated approach could be attempted where the isochrones are identified for example through contrast. This could be done for example with the spectral angle mapper (SAM), as presented by Naegeli et al. (2015). These approaches could lead to a more objective identification of the time series.

For further investigation on the absolute years, additional images, possibly showing a fresh event to determine an absolute year, could be gathered with more time. For this, announcements could be made in “die Alpen”, the magazine of the Swiss alpine club, or in the hut, and contact to the local community could be further established. Thereby, images from summer would be preferred, which poses another difficulty due to ski tourism being the main attraction at the Witenwasserengletscher. Moreover, the width of the isochrones could be used similarly to dendrochronology after eliminating topographic distortion. The curve of the isochrone widths would be compared to graphs of the temperature, glacial mass balance, or even tree ring widths, to assign it to a specific time.

On a glacier with an active accumulation area and visible isochrones, a ground penetrating radar (GPR) with a frequency of around 120 MHz (Gillespie et al., 2023; Guideline Geo AB, 2022; Sinisalo et al., 2003) could be used to identify isochrones in the accumulation area within the glacier. These isochrones could be traced to the surface of the glacier and then be used to confirm the years identified with the methods applied in this study and thus validate these methods. A similar approach could be done by using ice cores (cf. e.g. Sinnl et al., 2022; Winstrup et al., 2012). Rockfall deposits which are still inside the glacier and not melted out yet and therefore not visible on the surface could be detected with GPR as well. To do so frequencies between 50 and 100 MHz could be used depending on how long ago the events took place or how far below the glacier surface they are located (Dunning et al., 2015).

As precipitation can vary locally, an interpolation with different models could be done to get a more accurate image of the precipitation at the Witenwasserengletscher. This might give a different result for the comparison of heavy precipitation with rockfall occurrence. For a closer investigation of the influence of heavy precipitation on rockfall occurrence, examinations with higher temporal resolution should be conducted. Thereby, it would also be possible to look at specific criteria like one or more extremely warm days in combination with autumn snow, triggering a rockfall event as suggested by Allen & Huggel (2013).

For an in-depth understanding of the processes involved in rock wall instability and rockfall occurrence, variables included in the PERMOS database could be investigated further. The variables “glacier” and “permafrost” could be compared to each other (e.g. how many rockfall events have both, or none) or examined over time. Furthermore, other aspects of the events in the PERMOS database, such as the elevation or season, could be analysed and compared to these variables in literature and in the investigated rockfall events.

9 Conclusion

Between 1913 and 2014 27 rockfall events, with volumes between 0.05 and 561 m³, occurred from the headwall of the Witenwasserengletscher. This study shows that it is possible to reconstruct these events from melted out deposits on a glacier with the help of isochrones. Using the methods applied, a complete time series of rockfall events from a glacier's headwall over a period of several decades can be identified. For this the following conditions must be met:

- The investigated glacier must have an active accumulation area at the time the events occur.
- An active rock face must be present above the accumulation area of the glacier.
- Isochrones must be visible and intact.
- Aerial and/or drone images must be available and of sufficient quality.

The identification of rockfall events from isochrones on a glacier is not trivial and brings several uncertainties with it, including the identification and allocation of the isochrones, uncertainties in field measurements, and assigning absolute years to the time series, making the dating of the events challenging. Therefore, further studies would be needed to confirm the applied methods.

The study also showed that breakout zones of rockfall events can be determined from the geology identification in the field or streamline modelling. To achieve optimal results, these two approaches should be combined.

The temporal distribution of the detected events at Witenwasserengletscher matches well with the PERMOS rockfall database, especially when excluding the reporting bias. Further, a substantial connection between the rockfall occurrence and high temperatures was identified. Such events are therefore likely to increase with rising temperatures due to human-induced climate change. A relationship between heavy precipitation and rockfall occurrence could not be identified. To further investigate this connection, further research with higher temporal resolution is needed.

Literature

- Alberti, S., & Spreafico, M. C. (2019, April 29). *Natural Hazards | Alpine rock instability events and mountain permafrost*. EGU Blogs. <https://blogs.egu.eu/divisions/nh/2019/04/29/alpine-rock-instability-events-and-mountain-permafrost/>
- Allen, S., & Huggel, C. (2013). Extremely warm temperatures as a potential cause of recent high mountain rockfall. *Global and Planetary Change*, *107*, 59–69. <https://doi.org/10.1016/J.GLOPLACHA.2013.04.007>
- Ballantyne, C. K. (2002). Paraglacial geomorphology. *Quaternary Science Reviews*, *21*(18–19), 1935–2017. [https://doi.org/10.1016/S0277-3791\(02\)00005-7](https://doi.org/10.1016/S0277-3791(02)00005-7)
- Benn, D., & Evans, D. J. A. (2010). *Glaciers and Glaciation* (2nd ed.). Hodder Education. <https://doi.org/10.4324/9780203785010/GLACIERS-GLACIATION-2ND-EDITION-DOUGLAS-BENN-DAVID-EVANS>
- Bennett, M. R., & Glasser, N. F. (2009). Glacial Debris Entrainment and Transport. In *Glacial Geology: Ice Sheets and Landforms* (2nd ed., pp. 185–205). John Wiley & Sons.
- BGS (Bodenkundliche Gesellschaft der Schweiz). (2010). *Klassifikation der Böden der Schweiz – Bodenprofiluntersuchung, Klassifikationssystem, Definitionen der Begriffe, Anwendungsbeispiele*.
- Bolch, T., & Christiansen, H. H. (2015). Mountains, Lowlands, and Coasts: The Physiography of Cold Landscapes. In *Snow and Ice-Related Hazards, Risks, and Disasters* (pp. 201–217). Elsevier Inc. <https://doi.org/10.1016/B978-0-12-394849-6.00007-X>
- Bundesamt für Umwelt (BAFU). (2005). *Hinweiskarte der potenziellen Permafrostverbreitung* (Data State: 31.12.2011).
- Carey, M., McDowell, G., Huggel, C., Marshall, B., Moulton, H., Portocarrero, C., Provant, Z., Reynolds, J. M., & Vicuña, L. (2021). A socio-cryospheric systems approach to glacier hazards, glacier runoff variability, and climate change. In *Snow and Ice-Related Hazards, Risks, and Disasters* (pp. 215–257). Elsevier Inc. <https://doi.org/10.1016/B978-0-12-817129-5.00018-4>
- Cogley, J. G., Hock, R., Rasmussen, L. A., Arendt, A. A., Bauder, A., Braithwaite, R. J., Jansson, P., Kaser, G., Möller, M., Nicholson, L., & Zemp, M. (2011). *Glossary of glacier mass balance and related terms*. IHP-VII Technical Documents in Hydrology NO. 86, IACS Contribution No. 2, UNESCO-IHP. <http://www.unesco.org/water/ihp/>
- DATAtab. (n.d.). *Chi-Quadrat Verteilung Tabelle*. Retrieved April 21, 2024, from <https://datatab.de/tutorial/tabelle-chi-quadrat>
- Deline, P., Gruber, S., Delaloye, R., Fischer, L., Geertsema, M., Giardino, M., Hasler, A., Kirkbride, M., Krautblatter, M., Magnin, F., McColl, S., Ravel, L., & Schoeneich, P. (2015). Ice Loss and Slope Stability in High-Mountain Regions. In *Snow and Ice-Related Hazards, Risks, and Disasters* (pp. 521–561). Elsevier Inc. <https://doi.org/10.1016/B978-0-12-394849-6.00015-9>
- Dikau, R., & Glade, T. (2002). Gefahren und Risiken durch Massenbewegungen. *GR*, *54*, 38–45.
- Dobinski, W. (2011). Permafrost. *Earth-Science Reviews*, *108*(3–4), 158–169. <https://doi.org/10.1016/J.EARSCIREV.2011.06.007>

- Dunning, S. A., Rosser, N. J., McColl, S. T., & Reznichenko, N. V. (2015). Rapid sequestration of rock avalanche deposits within glaciers. *Nature Communications*, 6(1), 1–7. <https://doi.org/10.1038/ncomms8964>
- Evans, S. G., & Delaney, K. B. (2015). Catastrophic Mass Flows in the Mountain Glacial Environment. In *Snow and Ice-Related Hazards, Risks, and Disasters* (pp. 563–606). Elsevier Inc. <https://doi.org/10.1016/B978-0-12-394849-6.00016-0>
- Fairbridge, R. W., & Oliver, J. E. (2005). Lapse Rate. *Encyclopedia of Earth Sciences Series*, 448–450. https://doi.org/10.1007/1-4020-3266-8_123
- geo.admin.ch. (n.d.). Retrieved April 25, 2024, from <https://map.geo.admin.ch/>.
- Gervais, B. (2015). *Living Physical Geography* (C. Linsmeier, Ed.; 1st ed.). W. H. Freeman and Company.
- Gillespie, M. K., Yde, J. C., Andresen, M. S., Citterio, M., & Gillespie, M. A. K. (2023). Ice geometry and thermal regime of Lyngmarksbræen Ice Cap, West Greenland. *Journal of Glaciology*, 1–13. <https://doi.org/10.1017/JOG.2023.89>
- GIUZ (Department of Geography, University of Zurich (2022). *Drone Image from Witenwasserengletscher*.
- GIUZ (Department of Geography, University of Zurich (2023). *Drone Image from Witenwasserengletscher*.
- GLAMOS. (2023). *Swiss Glacier Volume Change, release 2023*. Glacier Monitoring Switzerland. <https://doi.org/10.18750/volumechange.2023.r2023>
- Goodsell, B., Hambrey, M. J., & Classer, N. F. (2005). Debris transport in a temperate valley glacier: Haut Glacier d'Arolla, Valais, Switzerland. *Journal of Glaciology*, 51(172), 139–146. <https://doi.org/10.3189/172756505781829647>
- Gruber, S., & Haeberli, W. (2007). Permafrost in steep bedrock slopes and its temperature-related destabilization following climate change. *Journal of Geophysical Research: Earth Surface*, 112, 2–18. <https://doi.org/10.1029/2006JF000547>
- Gruber, S., Hoelzle, M., & Haeberli, W. (2004). Permafrost thaw and destabilization of Alpine rock walls in the hot summer of 2003. *Geophysical Research Letters*, 31(13). <https://doi.org/10.1029/2004GL020051>
- Guideline Geo AB. (2022, January 10). *How can I do a velocity calibration for my GPR investigation?* <https://www.guidelinegeo.com/help-articles/what-antenna-frequency-should-i-use-for-my-gpr-investigation/>
- Haeberli, W., Huggel, C., Paul, F., & Zemp, M. (2013). 13.10 Glacial Responses to Climate Change. *Treatise on Geomorphology*, 1–14, 152–175. <https://doi.org/10.1016/B978-0-12-374739-6.00350-X>
- Haeberli, W., & Whiteman, C. (2015). Snow and Ice-Related Hazards, Risks, and Disasters: A General Framework. In *Snow and Ice-Related Hazards, Risks, and Disasters* (pp. 1–34). Elsevier Inc. <https://doi.org/10.1016/B978-0-12-394849-6.00001-9>
- Hafner, S., Günthert, A., Burckhardt, C. E., Steiger, R. H., Hasen, J. W., & Niggli, C. R. (1975). *Geologischer Atlas GA25 – 68 Val Bedretto (LK 1251)*.

<https://shop.swisstopo.admin.ch/de/karten/geologische-karten/geologischer-atlas-der-schweiz-25000>.

- Hammer, C. U. (1980). Acidity of Polar Ice Cores in Relation to Absolute Dating, Past Volcanism, and Radio-Echoes. *Journal of Glaciology*, 25(93), 359–372.
<https://doi.org/10.3189/S0022143000015227>
- Hess, H. (1902). Ueber den Zusammenhang zwischen Schichtung und Bänderung der Gletscher. *Neues Jahrbuch für Mineralogie, Geologie und Paläontologie*, 23–34.
- Hindmarsh, R. C. A., Leysinger Vieli, G. J. M. C., & Parrenin, F. (2009). A large-scale numerical model for computing isochrone geometry. *Annals of Glaciology*, 50(51), 130–140.
<https://doi.org/10.3189/172756409789097450>
- IPCC. (2007). *Synthesis Report. Contribution of Working Groups I, II and III to the Fourth Assessment Report of the Intergovernmental Panel on Climate Change* (Core Writing Team Pachauri R. K. and Reisinger, A., Eds.; p. 104). IPCC.
- IPCC. (2013). *Climate Change 2013: The Physical Science Basis. Contribution of Working group I to the Fifth Assessment Report of the Intergovernmental Panel on Climate Change* (C. Sabine, G. Bala, L. Bopp, V. Brovkin, J. Canadell, A. Chhabra, R. DeFries, J. Galloway, M. Heimann, C. Jones, C. Le Quéré, R. B. Myneni, S. Piao, & P. Thornton, Eds.; p. 1535). Cambridge University Press, Cambridge.
- IPCC. (2021). *Climate Change 2021: The Physical Science Basis. Contribution of Working Group I to the Sixth Assessment Report of the Intergovernmental Panel on Climate Change* (Masson-Delmotte, V., P. Zhai, A. Pirani, S. L. Connors, C. Péan, S. Berger, N. Caud, Y. Chen, L. Goldfarb, M. I. Gomis, M. Huang, K. Leitzell, E. Lonnoy, J. B. R. Matthews, T. K. Maycock, T. Waterfield, O. Yelekçi, R. Yu, & B. Zhou, Eds.; p. 2391). Cambridge University Press.
- Kenner, R. (2018). *Permafrost and Ground Ice Map of Switzerland*.
- Luckman, B. H. (2013). 7.17 Processes, Transport, Deposition, and Landforms: Rockfall. *Treatise on Geomorphology*, 1–14, 174–182. <https://doi.org/10.1016/B978-0-12-374739-6.00162-7>
- Mattson, L., Gardner, J., & Young, G. (2008). *Ablation on Debris Covered Glaciers: an Example from the Rakhiot Glacier, Punjab, Himalaya*.
- McCull, S. T. (2012). Paraglacial rock-slope stability. *Geomorphology*, 153–154, 1–16.
<https://doi.org/10.1016/J.GEOMORPH.2012.02.015>
- MeteoSchweiz. (2023). *Temperature and Precipitation Data*.
<https://gate.meteoswiss.ch/idaweb/login.do>
- Meyer, J. (2022). *Gesteine der Schweiz – Der Feldführer* (2nd ed.). Haupt Verlag.
- Naegeli, K., Damm, A., Huss, M., Schaepman, M., & Hoelzle, M. (2015). Imaging spectroscopy to assess the composition of ice surface materials and their impact on glacier mass balance. *Remote Sensing of Environment*, 168, 388–402. <https://doi.org/10.1016/J.RSE.2015.07.006>
- Nereson, N. A., Raymond, C. F., Waddington, E. D., & Jacobel, R. W. (1998). Migration of the Siple Dome ice divide, West Antarctica. *Journal of Glaciology*, 44(148), 643–652.
<https://doi.org/10.3189/S0022143000002148>

- Noetzli, J., Hoelzle, M., & Haeberli, W. (2003). *Mountain permafrost and recent Alpine rock-fall events: a GIS-based approach to determine critical factors*. In Phillips, M; et al. *Permafrost: proceedings of the eighth International Conference on Permafrost*. Lisse, The Netherlands (pp. 827-832). Balkema Publisher. <https://doi.org/https://doi.org/10.5167/uzh-33321>
- Ohmura, A. (2015). Snow and Ice in the Climate System. In *Snow and Ice-Related Hazards, Risks, and Disasters* (pp. 77–98). Elsevier Inc. <https://doi.org/10.1016/B978-0-12-394849-6.00003-2>
- PERMOS. (n.d.). *Rock Falls | PERMOS – Swiss Permafrost Monitoring Network*. Retrieved April 7, 2024, from <https://www.permos.ch/data-portal/rock-falls>
- PERMOS. (2023). *Permafrost rock fall database SLF/PERMOS*.
- Phillips, M. (2024a). *Personal Communication 25.03.2024*.
- Phillips, M. (2024b). *Personal Communication 26.02.2024*.
- PLANAT (Nationale Plattform Naturgefahren). (n.d.). *Steinschlag und Felssturz*. Retrieved February 11, 2024, from <https://www.planat.ch/de/wissen/rutschung-und-felssturz/steinschlag-/felssturz>
- Post, A., & Lachapelle, E. R. (2000). Ogives. In *Glacier Ice* (Revised Edition, pp. 61–73). University of Washington.
- Ravel, L., & Deline, P. (2010). Climate influence on rockfalls in high-Alpine steep rockwalls: The north side of the Aiguilles de Chamonix (Mont Blanc massif) since the end of the ‘Little Ice Age.’ *The Holocene*, 21(2), 357–365. <https://doi.org/10.1177/0959683610374887>
- Ravel, L., Magnin, F., & Deline, P. (2017). Impacts of the 2003 and 2015 summer heatwaves on permafrost-affected rock-walls in the Mont Blanc massif. *Science of The Total Environment*, 609, 132–143. <https://doi.org/10.1016/J.SCITOTENV.2017.07.055>
- Sinisalo, A., Grinsted, A., Moore, J. C., Kärkäs, E., & Pettersson, R. (2003). Snow-accumulation studies in Antarctica with ground-penetrating radar using 50, 100 and 800 MHz antenna frequencies. *Annals of Glaciology*, 37, 194–198. <https://doi.org/10.3189/172756403781815825>
- Sinnl, G., Winstrup, M., Erhardt, T., Cook, E., Jensen, C. M., Svensson, A., Vinther, B. M., Muscheler, R., & Rasmussen, S. O. (2022). A multi-ice-core, annual-layer-counted Greenland ice-core chronology for the last 3800 years: GICC21. *Climate of the Past*, 18(5), 1125–1150. <https://doi.org/10.5194/CP-18-1125-2022>
- SLF. (n.d.). *Bergsturz, Steinschlag und Co.: FAQ und Dossier*. Retrieved April 14, 2024, from <https://www.slf.ch/de/naturgefahren/bergsturz-steinschlag-und-co-faq-und-dossier/>
- Street, R. B., Melnikov, P. I., Riseborough, D., Anisimov, O., Guodong, C., Lunardini, V. J., Gavrilova, M., Köster, E. A., Koerner, R. M., Meier, M. F., Smith, M., Baker, H., Grave, N. A., Clapperton, C. M., Brugman, M., Hodge, S. M., Menchaca, L., Judge, A. S., Quilty, P. G., ... Sayles, F. (1990). Seasonal snow cover, ice and permafrost. In *Climate Change - The IPCC Impact Assessment* (pp. 7-7–7-15).
- Streletskiy, D., Anisimov, O., & Vasiliev, A. (2015). Permafrost Degradation. In *Snow and Ice-Related Hazards, Risks, and Disasters* (pp. 303–344). Elsevier Inc. <https://doi.org/10.1016/B978-0-12-394849-6.00010-X>
- Swisscovery. (n.d.). *ETH-Bibliothek @ swisscovery - - witenwassereren*. Retrieved April 14, 2024, from <https://eth.swisscovery.slsp.ch/discovery/search?query=any,contains,witenwassereren&filter=rt>

ype,exact,images&tab=discovery_network&search_scope=DiscoveryNetwork&vid=41SLSP_ETH:ETH&offset=0

- swisstopo. (n.d.). *Swiss Map Raster 25*. <https://www.swisstopo.admin.ch/de/landeskarte-swiss-map-raster-25>. Bundesamt für Landestopografie swisstopo.
- swisstopo. (2018). *swissALTI3D Stand 2018*. Bundesamt für Landestopografie swisstopo.
- swisstopo. (2022). *SWISSIMAGE*. <https://www.swisstopo.admin.ch/de/geodata/images/ortho.html>. Bundesamt für Landestopografie swisstopo.
- v. Elverfeldt, K., Glade, T., & Dikau, R. (2008). *Naturwissenschaftliche Gefahren- und Risikoanalyse* (pp. 31–46).
- Wastl, C., & Zängl, G. (2008). Analysis of mountain-valley precipitation differences in the Alps. *Meteorologische Zeitschrift*, *17*(3), 311–321. <https://doi.org/10.1127/0941-2948/2008/0291>
- Wieczorek, G. F., & Jäger, S. (1996). Triggering mechanisms and depositional rates of postglacial slope-movement processes in the Yosemite Valley, California. *Geomorphology*, *15*(1), 17–31. [https://doi.org/10.1016/0169-555X\(95\)00112-1](https://doi.org/10.1016/0169-555X(95)00112-1)
- Winstrup, M., Svensson, A. M., Rasmussen, S. O., Winther, O., Steig, E. J., & Axelrod, A. E. (2012). Climate of the Past An automated approach for annual layer counting in ice cores. *Clim. Past*, *8*, 1881–1895. <https://doi.org/10.5194/cp-8-1881-2012>
- Zängl, G., Aulehner, D., Wastl, C., & Pfeiffer, A. (2008). Small-scale precipitation variability in the Alps: Climatology in comparison with semi-idealized numerical simulations. *QUARTERLY JOURNAL OF THE ROYAL METEOROLOGICAL SOCIETY Q. J. R. Meteorol. Soc.*, *134*(6), 1865–1880. <https://doi.org/10.1002/qj.311>

Appendix

Figures and Pictures

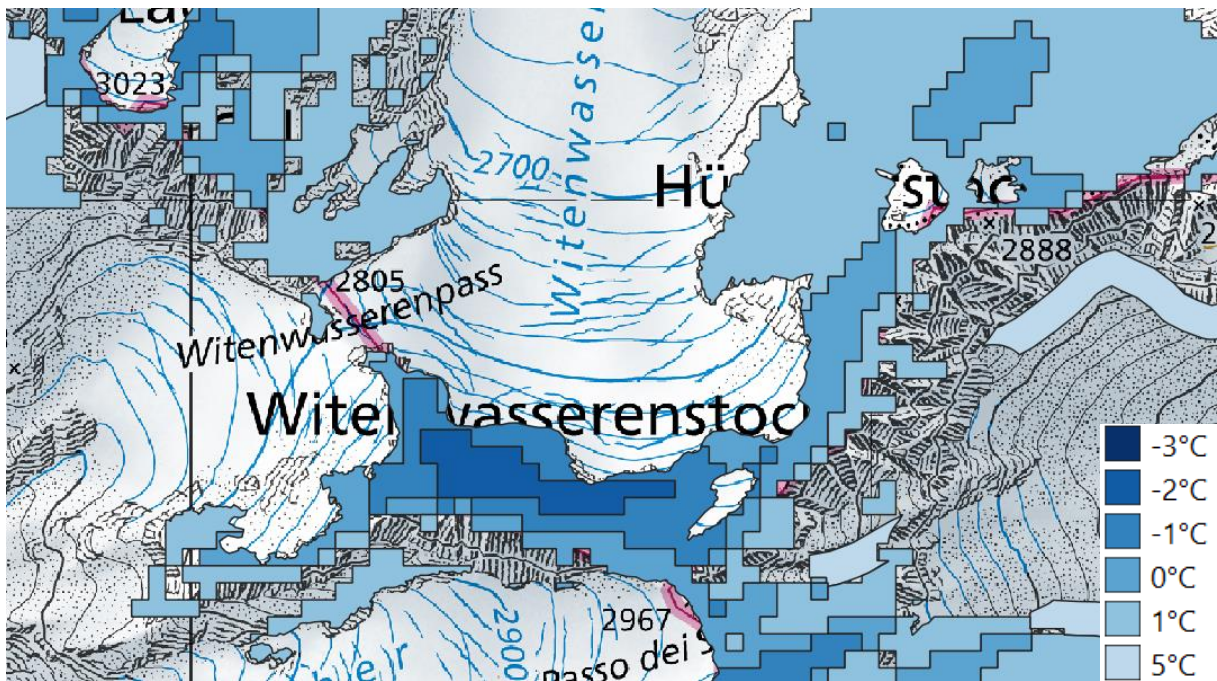


Figure A. 1: Permafrost distribution in the surrounding of the Witenwasserengletscher according to Kenner (2018) (background map: Swisstopo, n.d.).

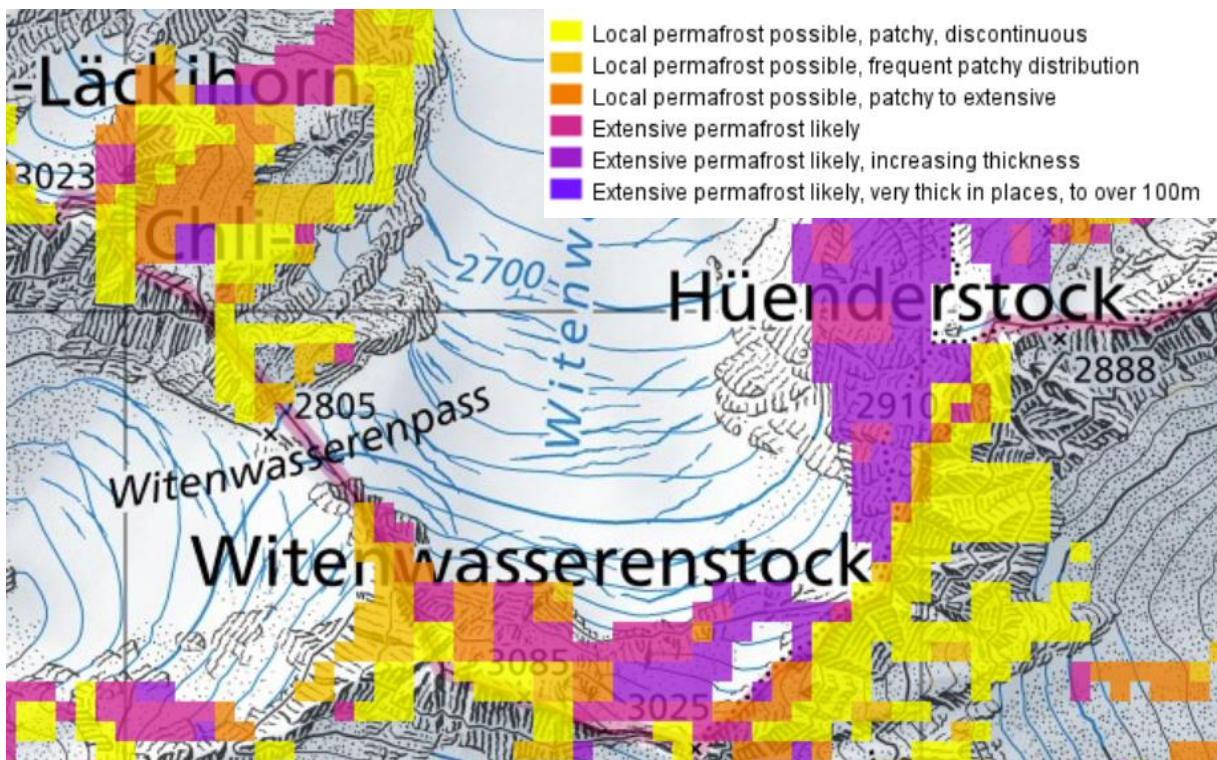


Figure A. 2: Permafrost distribution in the surrounding of the Witenwasserengletscher according to Swisstopo (BAFU, 2005; background map: Swisstopo, n.d.).

Figure A. 3: Pictures of the squares investigated in the field which were allocated to a deposit in the GIS, including the deposit name and measurement name.

A4 – Me5



A6 – Me29



A9 – Me35



A9 – Me38



A12 – Me32



A12 – Me34



A13 – Me28



A15 – Me27



A18 – Me8



A18 – Me23



A19 – Me25



A20 – Me1



A20 – Me2



A20 – Me3



A20 – Me24



A21 – Me6



A21 – Me7



A22 – Me9



A22 – Me10



A23 – Me19



A24 – Me18



A25 – Me15



A26 – Me17



A17 – Me13



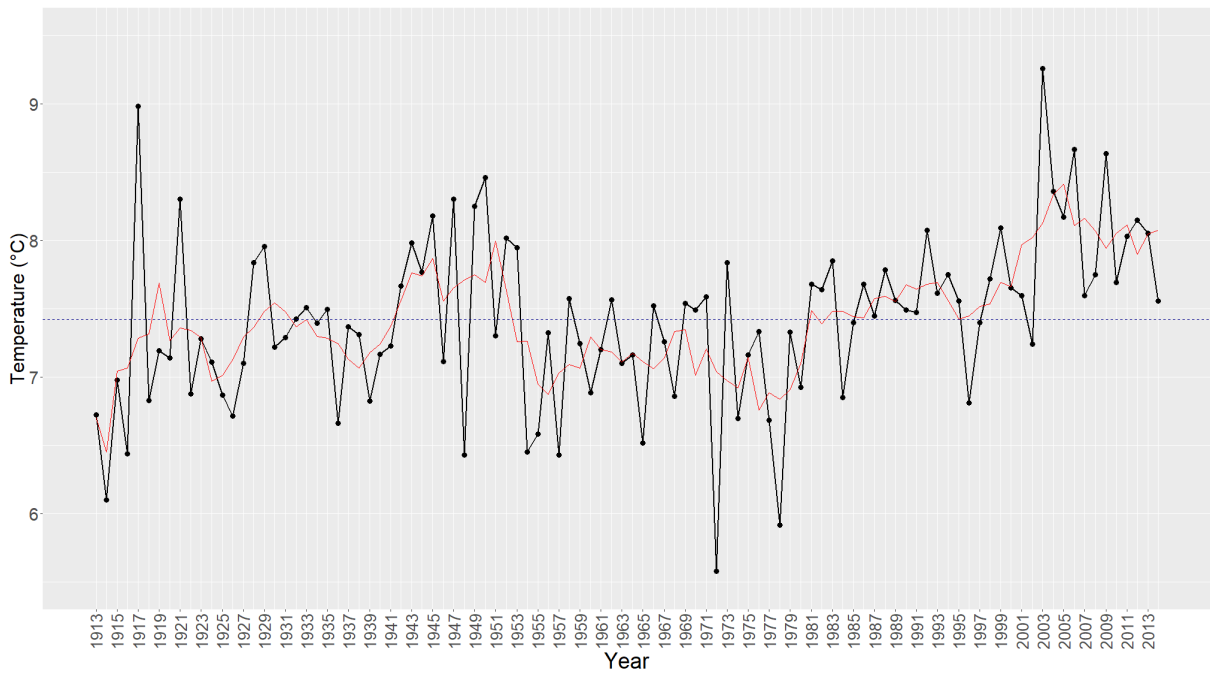


Figure A. 4: Annual mean temperature at the station in Andermatt from 1913 to 2014 with a mean over the displayed period (= 7.42 °C; blue dashed line) and a running mean (red) with $k = 5$ a (data: MeteoSchweiz, 2023).

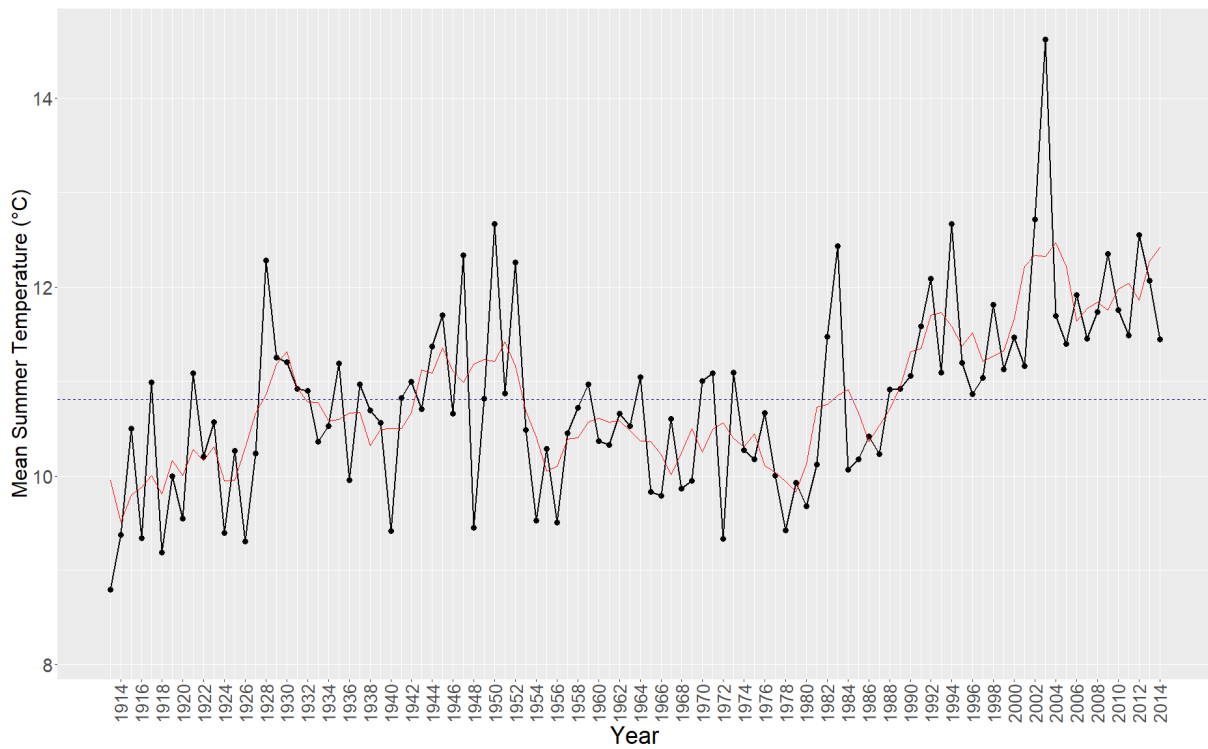


Figure A. 5: Mean summer temperature at the station in Andermatt from 1913 to 2014 with a mean over the displayed period (= 10.81 °C; blue dashed line) and a running mean (red) with $k = 5$ a (data: MeteoSchweiz, 2023).

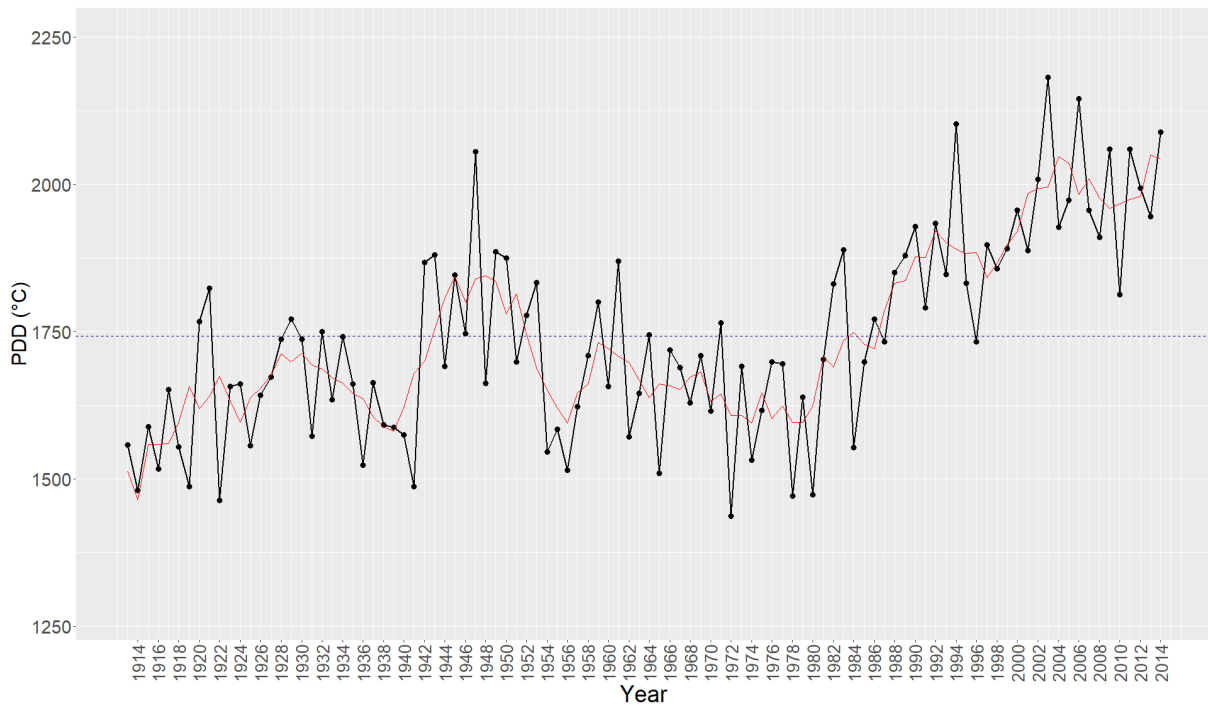


Figure A. 6: Positive degree day at an elevation of 3000 m a.s.l.(lapse rate = 0.6 °C per 100 m) with a mean over the displayed period (= 1742.16 °C; blue dashed line) and a running mean (red) with $k = 5$ a (data: MeteoSchweiz, 2023).

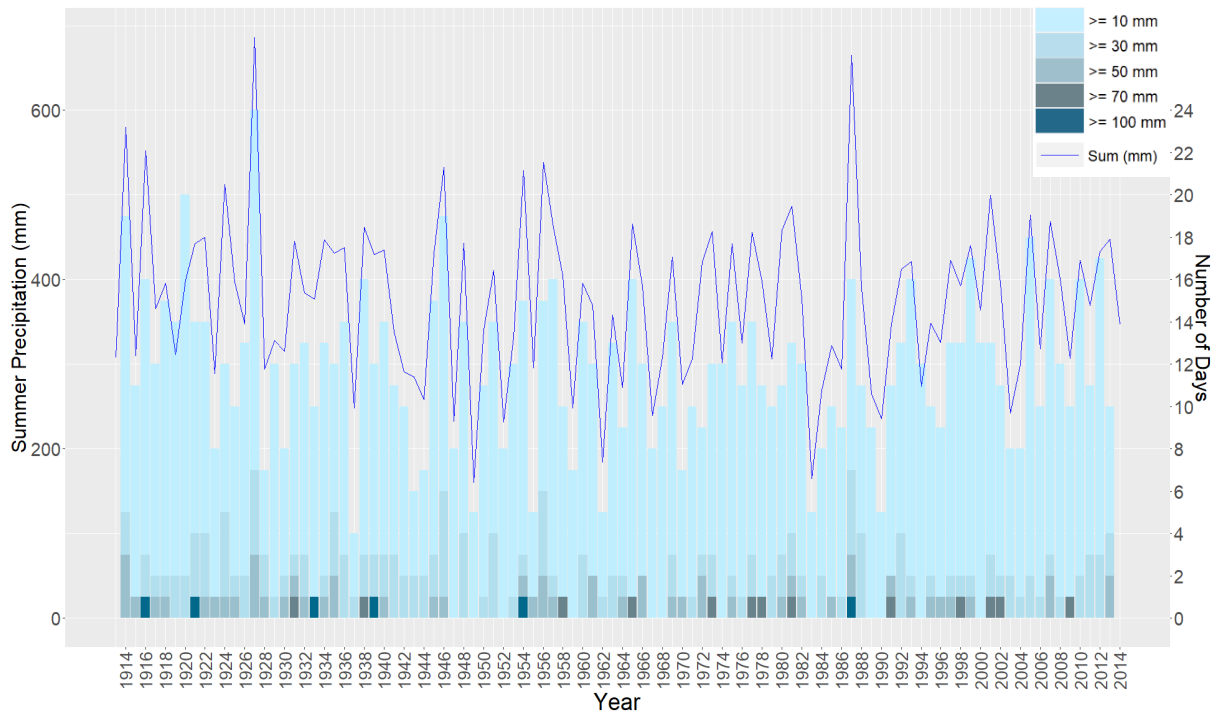


Figure A. 7: Summer precipitation in Andermatt from 1913 to 2014. Sum of summer precipitation (mm) and number of days with particularly large amounts of rain (data: MeteoSchweiz, 2023).

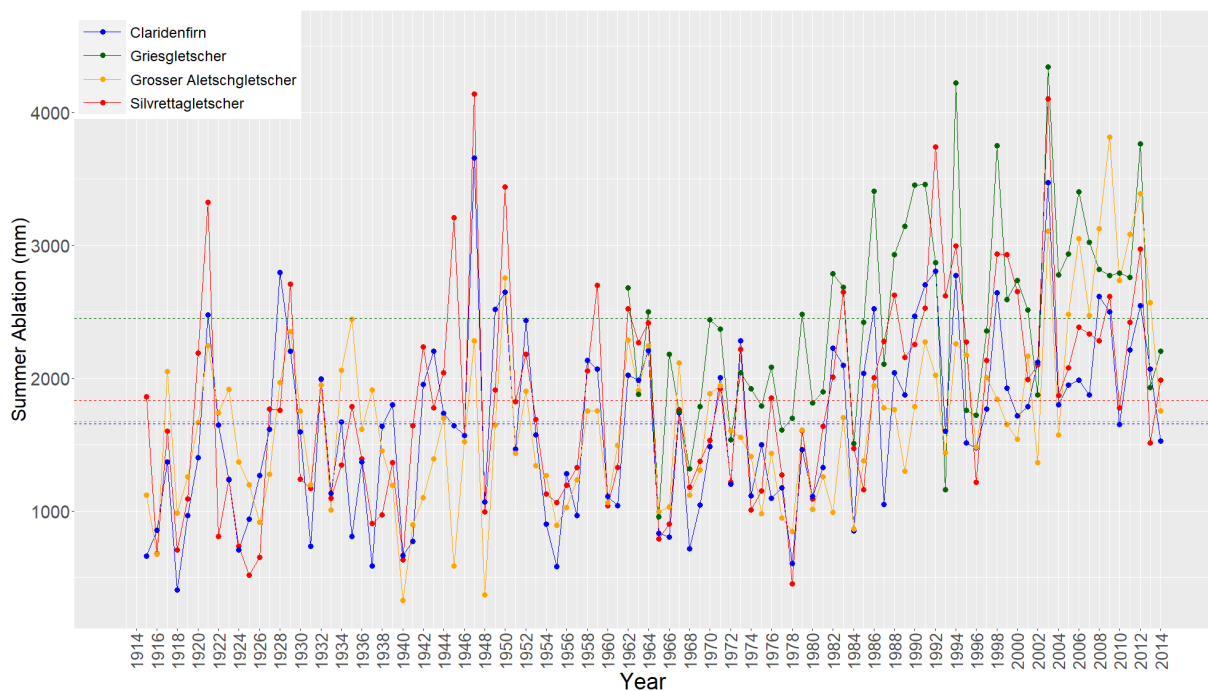


Figure A. 8: Summer mass balance of the Claridenfirn, Griesgletscher, Silvrettagletscher and Grosser Aletschgletscher, each with the mean value (dashed lines) from the beginning of their measurement to 2014 (data: GLAMOS, 2023).

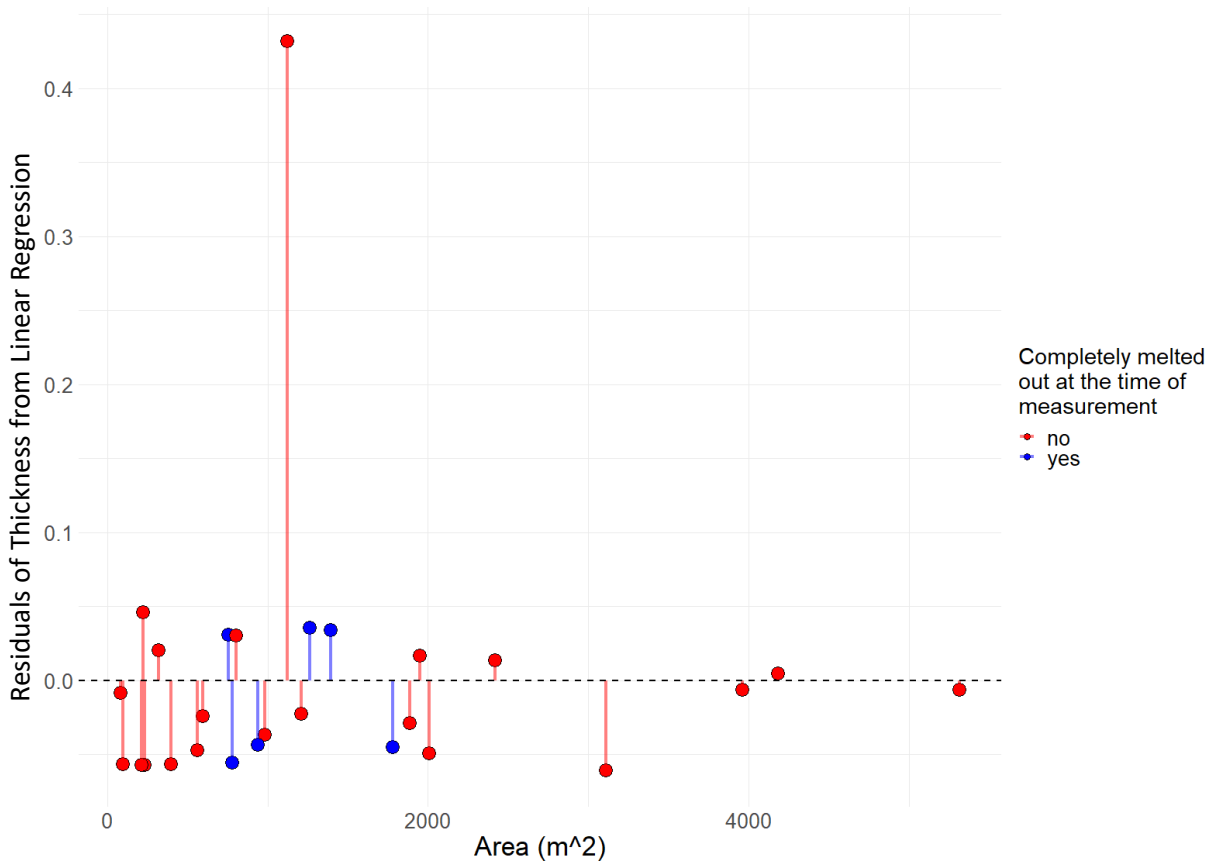


Figure A. 9: Residual diagram of the linear regression of the area and thickness.

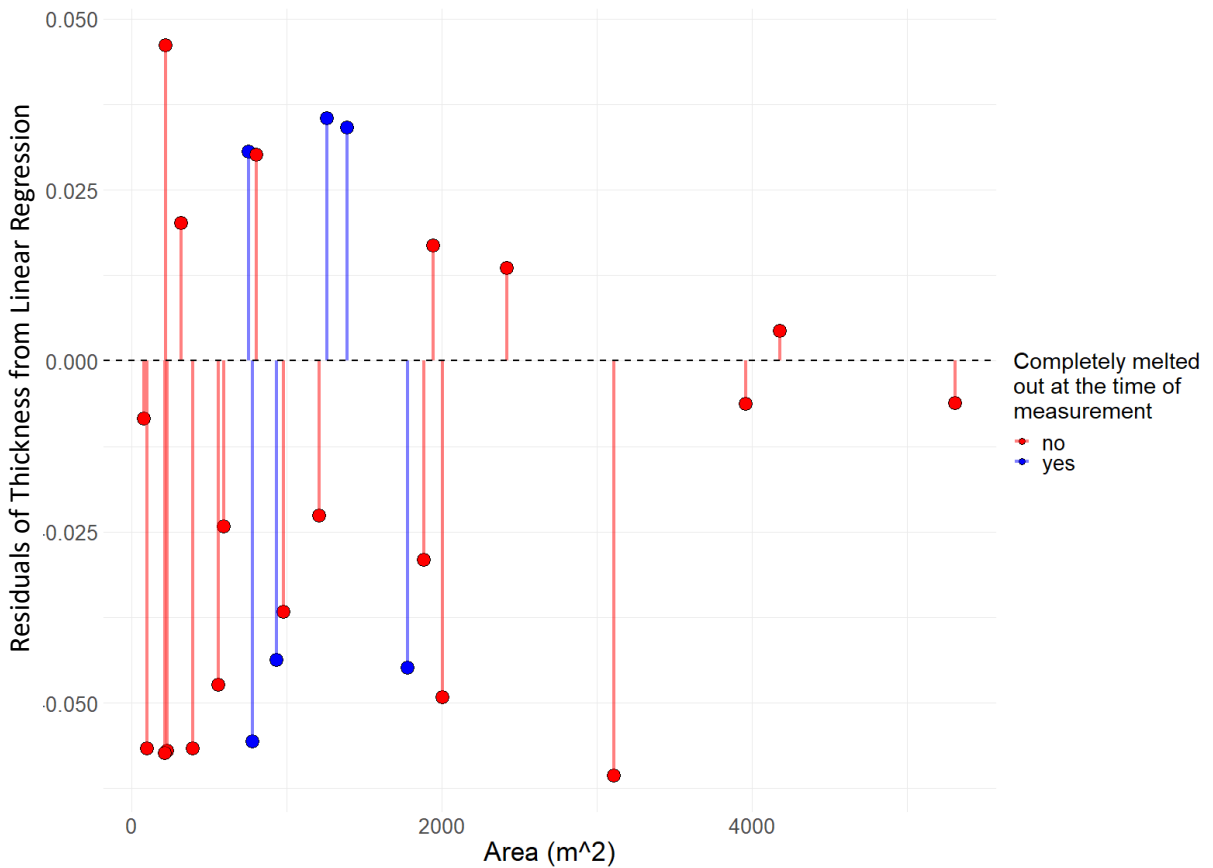


Figure A. 10: Residual diagram of the linear regression of the area and thickness without the outlier with a thickness of 0.5 m.

Tables

Table A. 1: Notes and remarks during the identification of the deposits on the Witenwasserengletscher on the drone image from 2022 (GIUZ, 2022).

Deposit	Approx. Melted out Area (m ²) (rounded in 10)	Clear Edge on Isochrone?	Observations
D_A_2022	850	no	
D_B_2022	1180	no	
D_C_2022	2710	no	Thin and spread over a large area. Lays between A & B → other geology?, maybe no rockfall deposit
D_D_2022	2030	yes	Not so clear where the deposition ends & the moraine starts
D_E_2022	1310	yes	Not so clear what belongs to E and what to F; only dense part measured
D_F_2022	1310	yes	Only dense part measured
D_G_2022	460	yes	
D_H_2022	690	No?	
D_I_2022	1180	yes	Not so clear where the deposition ends & the moraine starts
D_J_2022	240	no	Rockfall?
D_K_2022	40	no	Rockfall?, very small
D_L_2022	320	yes	Very thin
D_M_2022	1130	yes	End not so clear (downstreams)
D_N_2022	1250	Yes?	
D_O_2022	320	yes	
D_P_2022	1120	Yes?	
D_Q_2022	1940	yes	
D_R_2022	120	no	
D_S_2022	4400 (cutouts were not subtracted)	no	This seems to be a deposit from this / last year; widely spread, but not very dense
D_T_2022	810	No	Looks fresh
D_U_2022	320	no	Quite big rocks, only few & small area
D_V_2022	1020	no	On the very top, looks very fresh

Table A. 2: Data acquired in the field and allocation of measurements to deposits identified in GIS (AX).

	X	Y	Höhe müM	Datum	Zeit Foto	Geologie	Sand	Bemerkungen	% Bedeckung	% >1m	% 50cm-1m	% 30-50cm	% 20-30cm	% 10-20cm	% 5-10cm	% <5cm	% Total	Dicke (cm)	Dicke Kies	Dicke Steine	Dicke Brocken	Dicke Durchschnitt
Me1 (A20)	679643	154450	2610	21.08.2023	15:12	Streifengneis			30	0	0	65	20	10	5 (zusammen mit <5cm)		95	0.5-30				
Me2 (A20)	679630	154420	2614	21.08.2023	15:35	Streifengneis			95	5	30	25	15	15	10 (zusammen mit <5cm)		90		1.5 bis 2		70	
Me3 (A20)	679620	154373	2625	21.08.2023	16:00	Streifengneis		sehr unterschiedliche Schmelze je nach Bedeckung / Block	80	80	10	5	0	3	2 (zusammen mit <5cm)		98		0.3 bis 1		80 bis 100	
Me4	679737	154530	2572	21.08.2023	17:16	Streifengneis, kleinere Steine (<10cm) verwittert			98	0	0	0	15	15	25	45	100		0.5			
Me5 (A4)	679727	154551	2569	21.08.2023	17:27	Streifengneis, (Tonschiefer?), kleinere verwittert	wenig Sand		70	0	0	5	5	15	30	45	100		1	20		
Me6 (A21)	679597	154311	2630	22.08.2023	10:10	Streifengneis			55	0	0	50	10	5	15	20	100		1 bis 1.5	20		
Me7	679606	154334	2624	22.08.2023	10:51	Streifengneis, Rotondogranit			95	0	50	40	8	1	1 (< 10cm)		99		0.5 bis 1	20 bis 40		
Me8 (A18)	679633	154289	2655	22.08.2023	12:58	Streifengneis	kaum Sand		75	0	0	8	8	14	70 (< 10cm)		30		1	15		
Me9 (A22)	679652	154199	2662	22.08.2023	13:24	Streifengneis	kein Sand		30	40	20	15	10	7.5	5	2.5	100		0.5	20	65	
Me10 (A22)	679653	154170	2659	22.08.2023	13:44	Streifengneis	kein Sand		85	0	5	5	20	5	25	40	100		3	10 bis 15		
Me11	679707	153996	2697	22.08.2023	14:22	Streifengneis		Verminderte Schmelze durch Bedeckung / Erhöhung	90	0	20	30	20	15	5	10	100		0.5 bis 2	5 bis 20		7
Me12	679704	153970	2733	22.08.2023	14:42	Streifengneis	kein Sand	Erhöhung (Ablagerung -> weniger Schmelze)	98	0	2.5	2.5	15	20	25	35	100		4	6 bis 10 (15)		5
Me13 (A27)	679561	154028	2690	22.08.2023	15:27	Streifengneis	kein Sand		35	0	25	15	10	20	10	20	100		1	20		
Me14 (A27)	679565	154065	2683	22.08.2023	15:40	Streifengneis	kaum Sand	Einige Blöcke (1-2m) auf Ablagerung	99	10	15	10	20	15	15	15	100		3 bis 5	15 bis 45		10
Me15 (A25)	679581	154089	2672	22.08.2023	16:01	Streifengneis		Erhöhung durch verminderte Schmelze durch Ablagerung	100	2.5	22.5	30	20	10	5	10	100					50
Me16	679584	154345	2626	23.08.2023	10:18	Streifengneis		steil	15	0	35	25	15	10	10	5	100		0.3	10 bis 15	30	

Me17 (A26)	679552	154129	2658	23.08.2023	10:36	Streifengneis	kein Sand	ziemlich regelmässige Schmelze, ausser unter grossem Stein. Zwischen Steinen fliesst Wasser & mehr Schmelze	80	0	15	20	20	10	20	15	100	1 bis 2	10 bis 15	40			
Me18 (A24)	679517	154254	2645	23.08.2023	11:00	Rotondogranit		Stellenweise Sand, Kies mehr Steine (z.T. > 1m). Unter grossen Steinen mehr Eis, kleinere Steine vertieft / eingeschmolzen	30	0	90	0	7	2	1 (< 20cm)	0	99				kleine 2 bis 5, grosse 10 bis 35		
Me19 (A23)	679585	154269	2648	23.08.2023	11:16	Streifengneis	auch ganz fein		30	0	0	40	30	15	7.5	7.5	100	0.5 bis 2			grössere 15 bis 25, kleinere 2 bis 10		
Me20	679688	154250	2638	23.08.2023	11:36	Streifengneis	auch ganz fein	weniger Schmelze unter grossen Steinen	25	10	69	10	2.5	5	2.5	1	100				kleine 2, grosse 10 bis 35		
Me21	679703	154268	2634	23.08.2023	11:57	Streifengneis	(fast) kein Sand		55	0	48	26	10	10	5	1	100	0.5 bis 1			kleine 2-5, grosse 10-30		
Me22	679709	154387	2640	23.08.2023	12:13	Streifengneis, Oberstafelgneis	wenig Sand	z.T. gleichmässiger kleinere Steine -> verminderte Schmelze. Z.T. grössere Steine vereinzelter (50cm - 1m)	85	0	15	15	25	20	15	10	100	0.5 (bis 1)			5 bis 10	35	
Me23 (A18)	679634	154302	2640	23.08.2023	12:38	Streifengneis	wenig Sand	auf Ablagerung einige Blöcke > 1m, einige "rostige" Steine (< 20cm)	15	0	20	30	15	15	5	15	100	1.5			2 bis 15		
Me24 (A20)	679620	154360	2632	23.08.2023	13:37	Streifengneis (Granit?)		Teil der Ablagerung dichter (fast 100% bedeckt), einige grosse (>1m, 50-1m & 30-50)	90	20	15	15	15	15	15	5	100	1.5			5 bis 15	25	10
Me25 (A19)	679613	154377	2629	23.08.2023	13:53	Streifengneis	kaum/kein Sand	Kies Ansamung unter Steinen in "Steinschatten"	30	0	50	20	10	10	5	5	100	1.5				7	
Me26	679652	154468	2603	23.08.2023	14:17	Streifengneis (rostig)			25	80	0	5	7	1	2	5	100	0.5 bis 2.5			3 bis 8	60	
Me27 (A15)	679724	154603	2568	23.08.2023	14:40	Streifengneis, (Granit)			35	40	25	12.5	7.5	2.5	7.5	5	100	0.2 bis 1.5 (durchschnitt 1)			2 bis 20	17.5	
Me28 (A13)	679730	154646	2558	23.08.2023	15:10	Granit (grosse Blöcke), Streifengneis		weiter unten grössere Brocken (>1m, >2m Granit)	70	35	10	15	5	15	10	10	100	1 bis 1.5			3 bis 15	48	23
Me29 (A6)	679788	154671	2550	23.08.2023	15:50	Streifengneis, (Granit)			95	0	12.5	10	15	32.5	25	5	100	1.5 bis 2				10	

Me30	679715	154303	2636	24.08.2023	09:44	Streifengneis, Oberstafelgneis, (kleine Granite)	auch Sand		20	45	15	15	10	8	5	2	100		sehr dünn, 0.5	3 bis 16	20 bis 30	
Me31	679687	154354	2624	24.08.2023	10:08	Streifengneis		unter Block ausgeschmolzen -> Gletschertisch, unregelmässige Schmelze (eingelagerte Steine in Loch (mehrere zusammen))	75	65	10	10	7.5	4	1	2.5	100		0.2 bis 2	4 bis 20	50	20
Me32 (A12)	679704	154406	2607	24.08.2023	10:29	Streifengneis		unregelmässig geschmolzen, Gletschertische	55	40	20	10	5	10	5	10	100		0.5 bis 2	2 bis 10, grosse 5 bis 25	60	
Me33	679729	154390	2606	24.08.2023	10:50	Streifengneis, (Granit)		kein Kies, Erhöhung durch verminderte Schmelze durch Bedeckung. Innerhalb Bedeckung etwas unregelmässige Schmelze, aber nicht extrem. Bei grösseren Steinen (>30cm) etwas erhöht, bei kleineren (<30cm) regelmässig. Weiter unten z.T. etwas grössere Blöcke (nicht viele)	80	0	25	10	20	15	20	10	100		1.5	5-10cm = 3cm dick, 30 cm bis 1m = 20cm dick, Steine Durchschn. 6cm (10-30cm gross)		
Me34 (A12)	679722	154446	2586	24.08.2023	11:19	Streifengneis	kein Sand		65	50	15	10	5	7	3	10	100		1	5-30 gross = 5cm dick, 30- 50 = 15cm dick, > 1m = 40cm dick, 50-1m = 10cm dick		
Me35 (A9)	679737	154502	2572	24.08.2023	11:37	Streifengneis	kein Sand		75	25	25	20	5	10	5	10	100		1.5	5-20 = 4cm, 20-50 = 7cm, 50-1 = 35cm, >1m = 30cm		
Me36	679702	154495	2583	24.08.2023	11:55	Streifengneis	kaum Sand	steil an Seite runter, "Kamm", schmal	80	25	0	7.5	15	7.5	30	15	100		1.5 bis 2	5-20 = 6cm, 20-50 cm = 13, >1m = 50cm hoch (& 50cm breit)		
Me37	679716	154525	2585	24.08.2023	12:06	Streifengneis		"Grat / Kamm", schmal	98	0	0	15	5	10	10	60	100		2.5	5-30 = 3.5cm, 30-50 = 15cm		
Me38 (A9)	679726	154484	2497	24.08.2023	12:14	Streifengneis		Kies stellenweise sehr dünn, einzeln grössere Steine / Blöcke vermindern Schmelze, sonst ziemlich regelmässig	45	0	20	5	5	5	10	55	100		1.5, durch- schnitt 0.8	5-20 = 2.5cm, 30-50 = 10cm, 50-1m = 20cm		
Beobachtung Leonora & andere im Feld: Läckihorn rumpelt (mehrmals) täglich (in dieser Woche), von Gletscher aus gehört																						

Table A. 3: Notes from the interview with Pia Biondi (warden of the Rotondo hut) on 23.08.2023.

- keine bekannten Ereignisse
- v.a. letzte 2-3a rumpelns, vom Witenwasserstock
- seit 2022 ausapern, auch zwischen Läckihörnern (Eisfeld)
- Häufigkeit Rumpeln: fast täglich, mal mehr mal weniger
- Gefühl Zunahme von Jahr zu Jahr, auch Intensität/länger (hören), vorher nur einzelne Steine
- Eisschollen, neu, immer grösser & mehr (seit 2-3a)
- 2020 Änderungen (Eisschollen, mehr rumpeln)
- immer grüner (Richtung Läckipass)
- auch unter Hütte immer grüner, weniger loses Geröll
- 2015 (Pia seit dann auf Hütte) weisser Gletscher oben, Schneefelder
- Gletscher wird immer kiesiger

Table A. 4: Contacts and archives for the search of historical photographs.

Enquiry Contact	Outcome
Swisstopo (n.d.) aerial images	No deposits found
Photo archive ETH (Swisscovery, n.d.)	No useful pictures
Warden of Rotondo hut	No pictures available
SAC Lägern (owner of Rotondo hut)	No response
Municipality Realp	No pictures available
Talmuseum Urseren	No pictures available

Table A. 5: Measured and calculated variables of the identified rockfall deposits. "Melted out" refers to the deposit being melted out at the time of the area measurement (1 = yes, 0 = no), the thickness is the mean thickness in the covered part. "Confidence" refers to the confidence of the thickness and percentage coverage (0 = freely estimated (low confidence), 1 = similar to measurement, 2 = measured (high confidence)). "Block" refers to the block size-based classification (1 = "very small", 2 = "rockfall", 3 = "blockfall") and the "confidence block" refers to the confidence these classes. The last three columns show the number of images the deposits are "with an isochrone", "melted out" and "with an isochrone, but unsure which one" respectively.

Name	Melted out	Volume Rounded	Volume	Area	Thickness (m)	Coverage (%)	Confidence	Block	Rockslide	Confidence Block	With Isochrone	Melted out	Isochrone Unclear
A1	0	558	557.76	5312	0.15	70	1	3	1	2	2	3	0
A2	0	230	229.805	2419	0.1	95	1	3	1	2	2	3	0
A3	1	72	71.915	757	0.1	95	1	3	0	2	1	0	0
A4	0	1	0.3225	215	0.01	15	0	1	0	1	1	3	0
A5	0	4	4.116	84	0.05	98	1	2	0	2	2	1	1
A6	0	77	76.57	806	0.1	95	2	3	0	3	2	0	0
A7	0	24	23.52	224	0.14	75	1	3	0	2	2	3	0
A8	0	1	0.05	100	0.01	10	0	1	0	1	2	3	0
A9	1	133	132.51	1262	0.14	75	2	3	1	3	0	5	1
A10	0	435	434.824	4181	0.16	65	1	3	1	2	0	5	1
A11	1	7	7.038	782	0.03	30	0	2	0	1	1	1	0
A12	0	182	182.2315	1949	0.17	55	2	3	1	3	1	5	0
A13	1	146	146.16	1392	0.15	70	2	3	1	3	5	1	0
A14	0	2	1.596	399	0.02	20	0	3	0	2	1	1	0
A15	0	56	56.168	2006	0.08	35	2	3	0	3	5	1	0
A16	0	1	0.466	233	0.01	20	0	3	0	2	1	1	0
A17	0	29	29.46	982	0.12	25	2	3	0	3	1	2	0
A18	1	21	21.0825	937	0.03	75	2	2	0	3	1	2	0
A19	0	82	81.822	3112	0.1	28	2	3	0	3	2	0	0
A20	0	213	213.1185	3959	0.13	70	2	3	1	3	3	0	0
A21	0	23	22.9845	597	0.07	55	2	2	0	3	1	0	0
A22	0	49	48.6475	1212	0.08	58	2	3	0	3	2	0	0
A23	0	8	8.415	561	0.05	30	2	2	0	3	1	0	0
A24	1	53	53.43	1781	0.1	30	2	3	0	3	2	0	0
A25	0	561	560.5	1121	0.5	100	2	3	1	3	3	0	0
A26	0	26	25.76	322	0.1	80	2	3	0	3	1	0	0
A27	0	133	133.036	1889	0.07	67	2	3	1	3	3	0	0

Personal Declaration

I hereby declare that the submitted thesis is the result of my own, independent work. All external sources are explicitly acknowledged in the thesis.

Zürich, 29.04.2024



Leonora Seiler